Higher harmonics in gravitational wave signals from binary black hole mergers

Marien Hofstee

A thesis submitted to the Department of Gravitational and Subatomic Physics
at Utrecht University in partial fulfillment of the requirements for the degree of

Bachelor in Mathematics and Physics

supervisors: Prof. dr. C.F.F. van den Broeck
Dr. F.J. Ziltener
S. Roy

date of submission
16-06-2021

Universiteit Utrecht

Abstract

In the year 2019 two separate gravitational wave observations were done at the Virgo and LIGO detectors which were in both cases caused by two coalescing black holes of significantly different masses. These observations were GW190412 [Aea20a] and GW190814 [Aea20b]. In previous studies evidence was found for the prensence of higher harmonics in these black hole mergers [Aea20a]. This is also predicted by Einstein's General Relativity. By working out the first few orders of the gravitational waves, using the linearized Einstein equations and using data analysis on the observations, we can test general relativity in a new way to check if Einstein's predicitons were indeed correct. In this thesis we will work out the calculations and algorithms needed to do this test.

Additionally, we examinate the relation between higher harmonics in gravitational waves and spin-weighted spherical harmonics. We will find that the wavefunction can be written in terms of tensor spherical harmonics. Next, we prove that we can express the tensor harmonics in terms of spin-2 weighted spherical harmonics. This allows us in the end to find an equation for the waveform in terms of spin-2 weighted spherical harmonics.

Acknowledgments

I especially thank C.F.F. Van den Broeck and S. Roy for taking so much time for supporting me every week. I could not have wished for a better supervisor than Chris, who gave me tons of explanations. Likewise, Soumen guided me through the tough times of programming and data analysis.

Furthermore, I thank F.J. Ziltener for always being available when I needed him and giving me a lot of advice that was not only useful for this thesis, but will help me in future research as well.

Contents

1 Introduction

1.1 Motivation and main results

Ever since the first detection of gravitational waves in 2015 (GW150914) [BPA16], the progression in gravitational wave detection techniques and analysis has been booming. Since then all detections that were done included binary black holes or neutron stars with mass ratio's with a maximum of a factor two. Until in 2019 two observations were done of merging binary black holes with high relative mass difference. These were GW190412 [Aea20a] and GW190814 [Aea20b]. During GW190412 a black hole with a mass of $30M_\odot$ merging with a black hole with a mass of $8M_\odot$ was observed. While during GW190814 a black hole with a mass of $23M_\odot$ was observed merging with a compact object with a mass of $2.6M_\odot$.

This big relative mass difference allows us to test general relativity in a new way. As we can see in figure 1, during GW190412 not only the dominant harmonic was measurable, but also the harmonic that went with 1.5 times the frequency of the dominant harmonic was present in the observation. This is the first overtone in the waveform. We will calculate the waveform up until 0.5 Post-Newtonian order (PN) using the linearized Einstein Equations. Then we will look at data analysis techniques, like matched filtering and nested sampling, that we could use to test if the amplitudes of the different modes correspond with the data. In the end, we will set up a parameterized test to see if the amplitudes we calculated correspond with those found in the data. In this way we can test general relativity.

Additionally, as it turns out we can use spin-weighted spherical harmonics to express the waveform in different modes. After having defined the waveform in the transverse traceless gauge, we will look at the properties of tensor spherical harmonics as a basis. Then we will use the relation between tensor and spin-weighted spherical harmonics to in the end express the waveform in terms of spin-2 weighted spherical harmonics. The expression will take the following form

$$h = h_+ - ih_\times = \sum_{l=2}^{\infty} \sum_{m=-l}^{l} h^{lm}\, {}_{-2}Y^{lm}(\theta, \varphi). \tag{1.1}$$

Where h^{lm} are functions of the retarded time $t - \frac{r}{c}$. We will call $h^{lm}\, {}_{-2}Y^{lm}$ the l, m-mode.

1.2 Organization of this thesis

Section 2 contains some background material about how gravitiational waves are generated and how they can be described in the transverse traceless gauge, how we can detect them, and how they store energy. In Section 3 we will discuss the algorithms matched filtering

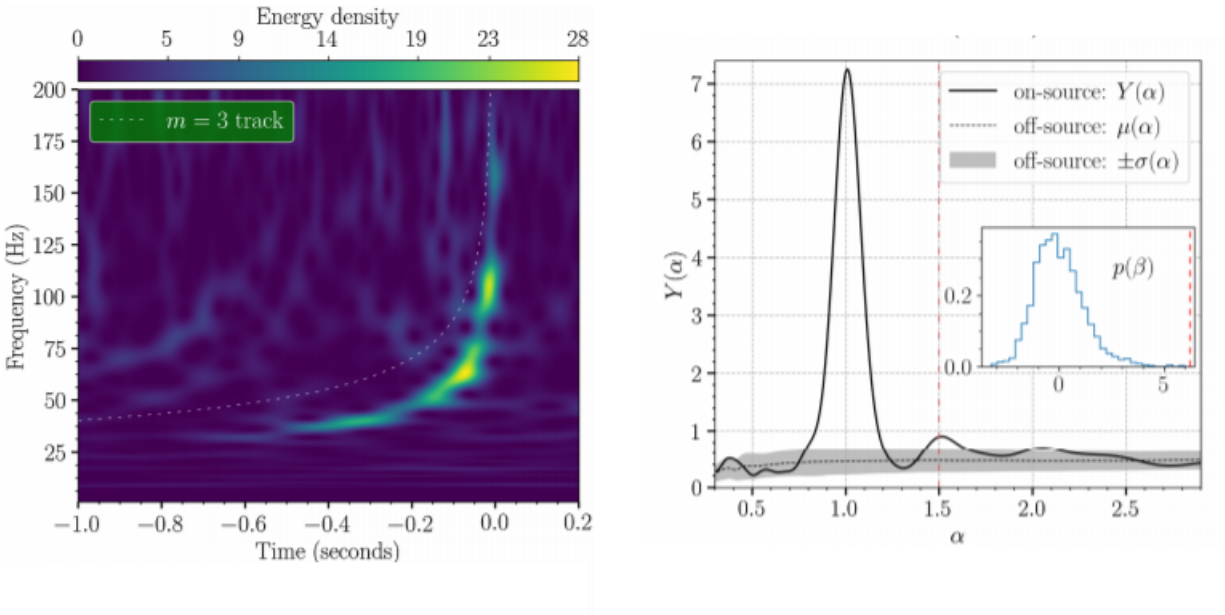

Figure 1: Left panel: The data of GW190412 is showed in a time-frequency spectrogram, which was observed in the LIGO Livingston detector. The horizontal axis represents time (in seconds) relative to the trigger time (1239082262.17). The dashed line shows the expected contribution of the $l = 3, m = 3$ mode. right panel: $Y(\alpha)$ represents the summed energy of the pixels on a path $f_\alpha(t)$ in the left panel. Here $f_\alpha(t)$ is defined as $\alpha f_{22}(t)$, where the f_{22} represents the $l = 2, m = 2$ mode from the IMRPhenomHM waverform. The peaks at $\alpha = 1.0$ and $\alpha = 1.5$ correspond to the $m = 2$ and $m = 3$ mode respectively. [Aea20a]

and nested sampling. We will need these later in section 7. In section 5, we will define the tensor and spin-weighted spherical harmonics and see how they are related to gravitational waves in the transverse traceless gauge. In Section 4, we will then use this to calculate the coefficient of eq. (1.1). In section 6, we will look at the python library PyCBC, and espacially the IMRPhenomHM waveform. We will need this library to set up our tests of general relativity explained in section 7. Finally, we will look at our simulated signals and the results in section 8.

2 Gravitational waves and their detection

In this section we will look at what gravitational waves are, namely a perturbation in space-time. We will use the linearized Einstein equations to find a solution given a source in the transverse traceless gauge. Then, we shall look at how energy is stored in gravitational waves, and how we can use this to detect them.

2.1 Linearized general relativity

In classical mechanics, Newtonian gravity works at an instant. Even if an object is some light years away, its movement and change of mass are immediately noticeable for an observer. In general relativity this works differently. Information is transfered with the speed of light c. In order to see this we will first derive the Linearized Einstein equations in this subsection.

In general relativity we make use of the metric tensor $g_{\mu\nu}$, which describes the curvature of spacetime. We can write this as

$$g_{\mu\nu} = \eta_{\mu\nu} + h_{\mu\nu}. \tag{2.1}$$

Here $\eta_{\mu\nu}$ is the Minkowski metric, and $h_{\mu\nu}$ is the perturbation term. General relativity allows us to make coordinate transformations $x'^{\mu}(x)$. If we use a coordinate transformation it will affect our metric tensor in the following way

$$g'_{\mu\nu} = \frac{\partial x^{\rho}}{\partial x'^{\mu}} \frac{\partial x^{\sigma}}{\partial x'^{\nu}} g_{\rho\sigma}. \tag{2.2}$$

Many coordinate transformations will make $h_{\mu\nu}$ large. Which means that the metric tensor differs a lot from the Monkowski metric. For simplicity we will assume that we are dealing with a weak field metric. This means that $|h_{\mu\nu}| \ll 1$. The consequence of this assumption is that this will restric the possibilities for our coordinate transformations. We are restricted to small transformations of the form

$$x'^{\mu} = x^{\mu} + \xi^{\mu}. \tag{2.3}$$

Here $\xi(x)$ does not have to be constant, however $\partial_{\nu}\xi^{\mu}(x)$ should be small. If we now use a transformation of the form in eq. (2.3) and fill this in into eq. (2.2) we will see that the new metric tensor becomes

$$g'_{\mu\nu} = (\frac{\partial x'^{\rho}}{\partial x'^{\mu}} - \frac{\partial \xi^{\rho}}{\partial x'^{\mu}})(\frac{\partial x'^{\sigma}}{\partial x'^{\nu}} - \frac{\partial \xi^{\sigma}}{\partial x'^{\nu}}) g_{\rho\sigma} = (\delta^{\rho}_{\mu} - \frac{\partial \xi^{\rho}}{\partial x'^{\mu}})(\delta^{\sigma}_{\nu} - \frac{\partial \xi^{\sigma}}{\partial x'^{\nu}})(\eta_{\rho\sigma} + h_{\rho\sigma}). \tag{2.4}$$

If we only consider terms which are linear in the small quantities, which in our case are $h_{\mu\nu}$ and derivatives of ξ^{ρ}, we can rewrite this to

$$g'_{\mu\nu} = \eta_{\mu\nu} + (h_{\mu\nu} - \partial_{\mu}\xi_{\nu} - \partial_{\nu}\xi_{\mu}) = \eta_{\mu\nu} + h'_{\mu\nu}. \tag{2.5}$$

Note that we replaced x' with x in the derivatives of ξ^μ. We can do this because extra terms that are being generated in this transformation are non linear in the small quantities.

Before we can fill the expression of our metric tensor into the Einstein equation we need to make a definition that will later turn out to be useful. We define $\bar{h}_{\mu\nu}$ by

$$\bar{h}_{\mu\nu} = h_{\mu\nu} + \frac{1}{2}\eta_{\mu\nu}h. \tag{2.6}$$

Where $h = \eta^{\mu\nu}h_{\mu\nu}$ is the trace. It transforms as

$$\bar{h}'_{\mu\nu} = \bar{h}_{\mu\nu} - (\partial_\mu\xi_\nu + \partial_\nu\xi_\mu - \eta_{\mu\nu}\partial_\rho\xi^\rho). \tag{2.7}$$

We can use this expression to help us find a solution for the Einstein Equation. The Einstein field equations are given by

$$G_{\mu\nu} = \frac{8\pi G}{c^4}T_{\mu\nu}. \tag{2.8}$$

In this equation $G_{\mu\nu}$ stands for the Einstein tensor, G is the gravitational constant, c the speed of light and finally $T_{\mu\nu}$ is the stress-energy tensor. We now substitute eq. (2.6) into eq. (2.8) to find

$$\Box\bar{h}_{\mu\nu} + \eta_{\mu\nu}\partial^\rho\partial^\sigma\bar{h}_{\rho\sigma} - \partial^\rho\partial_\nu\bar{h}_{\mu\rho} - \partial^\rho\partial_\mu\bar{h}_{\nu\rho} = -\frac{16\pi G}{c^4}T_{\mu\nu}. \tag{2.9}$$

Here $\Box$ is the d'Alembert operator. This is a waveoperator and it is defined as $\Box = \partial^\mu\partial_\mu$. We can now make use of the Lorentz gauge condition. The Lorentz gauge condition states that whatever $\bar{h}_{\mu\nu}$ is, there always exists a gauge transformation such that $\partial^\mu\bar{h}'_{\mu\nu} = 0$. This will simplify eq. (2.9) to

$$\Box\bar{h}_{\mu\nu} = -\frac{16\pi G}{c^4}T_{\mu\nu}. \tag{2.10}$$

2.2 General solution given a source

In the previous section we saw that by making the weak field assumption and using the Lorentz Gauge condition we can find a relation between gravitational waves and the stress-energy tensor. Now we need to find a solution for the wave equation if we are given a stress-energy tensor $T_{\mu\nu}$. In order to do so we will have to make use of the Green's function $\mathcal{G}(t, \mathbf{x})$ belonging to the d'Alembertian. This function has as a property that $\Box\mathcal{G}(t, \mathbf{x}) = \delta^4(t, \mathbf{x})$, where $\delta^4(t, \mathbf{x}) = \delta(t)\delta^3(\mathbf{x})$. Assuming that such a function exists, a solution is given by

$$\bar{h}_{\mu\nu}(t, \mathbf{x}) = -\frac{16\pi G}{c^4}\int dt'd^3\mathbf{x}'\, T_{\mu\nu}(t', \mathbf{x}')\mathcal{G}(t - t', \mathbf{x} - \mathbf{x}'). \tag{2.11}$$

Since then,

$$\begin{aligned}\Box\bar{h}_{\mu\nu}(t,\mathbf{x}) &= -\frac{16\pi G}{c^4}\int dt'd^3\mathbf{x}'\, T_{\mu\nu}(t',\mathbf{x}')\,\Box\mathcal{G}(t-t',\mathbf{x}-\mathbf{x}') \\ &= -\frac{16\pi G}{c^4}\int dt'd^3\mathbf{x}'\, T_{\mu\nu}(t',\mathbf{x}')\delta^4(t,\mathbf{x}) \\ &= -\frac{16\pi G}{c^4}T_{\mu\nu}. \end{aligned} \tag{2.12}$$

Now we just have to prove that such a Green's function exists. To do so we will first start with an ansatz that the function takes the form

$$\mathcal{G}(t,\mathbf{x}) = \frac{1}{r}F(t-\frac{r}{c}). \tag{2.13}$$

Where $r = |\mathbf{x}|$. Now we can use the property of the Green's function that $\Box\mathcal{G}(t,\mathbf{x}) = \delta^4(t,\mathbf{x})$. If we rewrite the d'Alembertian to

$$\Box = -\frac{1}{c^2}\frac{\partial^2}{\partial t^2} + \nabla^2, \tag{2.14}$$

and apply it to both sides of equation 2.13, then we find the relation

$$-4\pi F(t) = \delta(t). \tag{2.15}$$

What leaves us is to substitute this back into eq. (2.13) and this back into eq. (2.11). This gives us the final our solution to the wave equation, namely

$$\bar{h}_{\mu\nu}(t,\mathbf{x}) = \frac{4G}{c^4}\int dt'd^3\mathbf{x}' T_{\mu\nu}(t',\mathbf{x}')\frac{1}{|\mathbf{x}-\mathbf{x}'|}\delta(t-t'-\frac{|\mathbf{x}-\mathbf{x}'|}{c}). \tag{2.16}$$

Which simplifies to

$$\bar{h}_{\mu\nu}(t,\mathbf{x}) = \frac{4G}{c^4}\int_{\mathcal{V}} d^3\mathbf{x}'\frac{T_{\mu\nu}(t-\frac{|\mathbf{x}-\mathbf{x}'|}{c},\mathbf{x}')}{|\mathbf{x}-\mathbf{x}'|}. \tag{2.17}$$

Note that in this equation the integrand depends on the retarded time instead of the time. The retarded time is defined by $t_r = t - \frac{r}{c}$. This means that if the stress-energy tensor changes on time t inside the source, the observer which is a distance r away from the source only notices the change at time $t - \frac{r}{c}$. This contradicts the newtonian idea of gravity where changes are observable right away.

2.3 Transverse Traceless Gauge

Now we know how to find a solution for the wave inside of the source, we can look at what happens outside of the source. To see how gravitational waves travel outside of the source and to determine how they interact with test masses, it is useful to work in a gauge where

the wave is transverse to its travel direction, as well as where the wave has no trace. We call this the transverse traceless gauge [Mag08]. In this subsection we will look at how we can define this gauge and we will see that in this gauge the wave has only two degrees of freedom.

Outside of the source we have $T_{\mu\nu} = 0$, therefore also $\Box\bar{h} = 0$. By looking at eq. (2.7), the condition $\partial^\nu \bar{h}_{\mu\nu} = 0$ is not ruined by transformations $x^\mu \to x^\mu + \xi^\mu$ with $\Box\xi_\mu = 0$. This is true because

$$\partial^\nu(\partial_\mu\xi_\nu + \partial_\nu\xi_\mu - \eta_{\mu\nu}\partial_\rho\xi^\rho) = \Box\xi_\mu. \tag{2.18}$$

Now eq. (2.7) can help us to eliminate four of the six independent components of $\bar{h}_{\mu\nu}$ that satisfy $\Box\bar{h}_{\mu\nu} = 0$. We can substract the four independent functions ξ_μ, which also satisfy $\Box\xi_\mu = 0$, to impose the properties on $\bar{h}_{\mu\nu}$. We can choose ξ^0 such that the trace of $\bar{h}_{\mu\nu}$ equals zero. Note that if the trace is zero then $\bar{h}_{\mu\nu} = h_{\mu\nu}$. Furthermore, we can then choose $\xi^i(x)$ such that $h^{0i}(x) = 0$. Consequently, the Lorentz Gauge condition for $\mu = 0$ simplifies to

$$\partial^0 h_{00} + \partial^i h_{0i} = \partial^0 h_{00} = 0. \tag{2.19}$$

In other words, h_{00} is constant and does not contribute to the wave. This allows us to set $h_{00} = 0$. Therefore, we now set all $h_{0\mu}$ components to zero and are only left with the spatial components h_{ij}. The Lorentz Gauge condition therefore becomes $\partial^j h_{ij} = 0$. In conclusion we now have the following conditions

$$h^{0\mu} = 0,\ h^i_i = 0,\ \partial^j h_{ij} = 0. \tag{2.20}$$

These conditions define the transverse-traceless gauge (TT). The degrees of freedom for $h_{\mu\nu}$ have now been reduced from six to only two. This metric in the TT gauge will be denoted by h^{TT}_{ij}.

For a plane wave traveling in the direction $\hat{\mathbf{n}}$, the lorentz gauge condition can be rewritten to $\partial^j h^{TT}_{ij} = n^i h^{TT}_{ij}$. So the wave is transverse to the traveling direction. If we now choose $\hat{\mathbf{n}}$ in the z-direction, and choose our metric to be symmetric and traceless, then a simple waveform is

$$h^{TT}_{ij}(t,z) = \begin{pmatrix} h_+ & h_\times & 0 \\ h_\times & -h_+ & 0 \\ 0 & 0 & 0 \end{pmatrix} \cos[\omega(t - \frac{z}{c})]. \tag{2.21}$$

It turns out that there exists an opperator $\Lambda_{ij;kl}(\hat{\mathbf{n}})$ that projects the waveform that we found in eq. (2.17) to the waveform in the TT gauge [Mag08]. To define this opperator we first need to define another opperator

$$P_{ij}(\hat{\mathbf{n}}) = \delta_{ij} - n_i n_j. \tag{2.22}$$

As can be seen from the definition, P_{ij} is symmetric and transverse. Furthermore, it is a projector since $P_{ik}P_{kj} = P_{ij}$, and has a trace $P_i^i = 2$. We can use this to construct the TT gauge projector

$$\Lambda_{ij;kl}(\hat{\mathbf{n}}) = P_{ik}P_{jl} - \frac{1}{2}P_{ij}P_{kl}. \tag{2.23}$$

Note that this tensor is traceless, so both $\Lambda_{ii;kl} = \Lambda_{ij;kk} = 0$. Additionally, it is transverse in all indices, so $n^i\Lambda_{ij;kl} = 0$, $n^j\Lambda_{ij;kl} = 0$, etc. Now we need to show that this opperator indeed changes the wave to the transverse traceless gauge. Suppose that

$$h_{ij}^{TT} = \Lambda_{ij;kl}h_{kl}. \tag{2.24}$$

Due to the fact that $\Lambda_{ij;kl}$ is traceless and transverse it is clear that the righthand side of the equation is transverse and traceless. Secondly, because $\Box h_{kl} = 0$, it is still true that $\Box h_{ij}^{TT} = 0$. We conclude that indeed the waveform is projected onto the transverse traceless gauge. Our solution for the waveform now becomes

$$h_{ij}^{TT}(t, \mathbf{x}) = \frac{4G}{c^4}\Lambda_{ij;kl}(\hat{\mathbf{n}}) \int_{\mathcal{V}} d^3\mathbf{x}' \frac{T_{ij}(t - \frac{|\mathbf{x}-\mathbf{x}'|}{c}, \mathbf{x}')}{|\mathbf{x} - \mathbf{x}'|}. \tag{2.25}$$

2.4 Energy in gravitational waves

Now we know how the wave behaves outside the source we can focus on the energy that is stored in gravitational waves. Gravitational waves are caused by rotating heavy compact objects. In the process of inspiral, the distance between the objects becomes smaller. Subsequently, there is a loss of orbital energy. The loss in orbital energy is being transfered into the gravitational waves. Therefore, the system evolves according to the relation

$$-\frac{dE_{\text{orb}}}{dt} = \frac{dE_{\text{GW}}}{dt}. \tag{2.26}$$

Here E_{orb} is the orbital energy and $\frac{dE_{\text{GW}}}{dt}$ is the energy per time unit emitted in gravitational waves. In this subsection we will show that the energy per time unit emitted in gravitational waves is

$$\frac{dE_{\text{GW}}}{dt} = \frac{c^3r^2}{16\pi G} \int_{\mathcal{S}} d\Omega \, \langle \dot{h}_+^2 + \dot{h}_\times^2 \rangle. \tag{2.27}$$

To get to this expression we will follow the calculations done in [Mag08]. According to [Mag08], the fact that gravitational waves interact with test particles and that test particles can get kinetic energy from gravitational waves shows that gravitational waves do carry energy. General relativity states that any form of energy contributes to the curvature of space-time. Therefore, we will try to show that gravitational waves also contribute to the curvature.

Up until now we have linearized the Einstein equations by working with the flat metric $\eta_{\mu\nu}$ and the linear perturbations in them $h_{\mu\nu}$, which we called the gravitational waves.

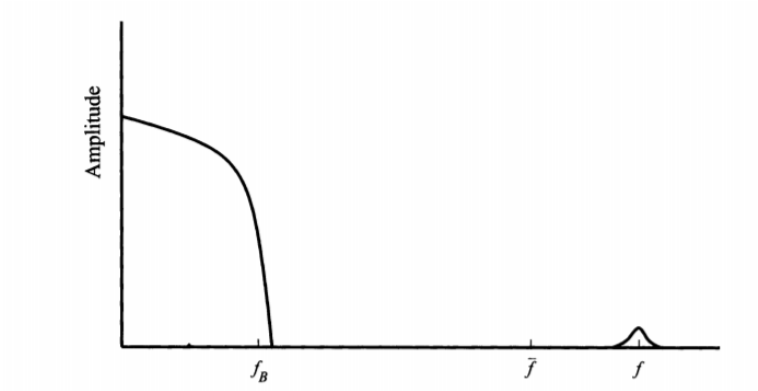

Figure 2: An example of a situation that lets us separate the metric in a low frequency background, and a high frequency gravitational wave metric [Mag08].

However, to find the result we are looking for this will not work, because in that case gravitational waves would always contribute to a curvature in space-time. Instead we need to define a dynamical background metric $\bar{g}_{\mu\nu}$, such that

$$g_{\mu\nu} = \bar{g}_{\mu\nu} + h_{\mu\nu}, \;\; |h_{\mu\nu}| \ll 1. \tag{2.28}$$

This immediately creates a problem: how do we know when a curvature is background and when it is a gravitational wave? This separation was simple when we linearized the metric, because the background was just flat and all curvatures were gravitational waves. Nevertheless, we can fairly easy solve this problem. Let's say that in the metric of eq. (2.28) $\bar{g}_{\mu\nu}$ has a maximum frequency of f_B. Whereas, $h_{\mu\nu}$ is peaked at f, such that

$$f_B \ll f. \tag{2.29}$$

In other words, $h_{\mu\nu}$ represents a quickly changing perturbation in a low frequency background. An example of such a situation is given in figure 2.

To start with, we need to expand to the quadratic order of $h_{\mu\nu}$. We can write the Einstein equation in the following form

$$R_{\mu\nu} = \frac{8\pi G}{c^4}(T_{\mu\nu} - \frac{1}{2}g_{\mu\nu}T). \tag{2.30}$$

In this equation $T_{\mu\nu}$ is the stress-energy tensor, and T is the trace of it. Next we expand the Ricci tensor $R_{\mu\nu}$ up until $O(h^2)$,

$$R_{\mu\nu} = \bar{R}_{\mu\nu} + R^{(1)}_{\mu\nu} + R^{(2)}_{\mu\nu} + \dots. \tag{2.31}$$

We defined $\bar{R}_{\mu\nu}$ with $\bar{g}_{\mu\nu}$ only, $R^{(1)}_{\mu\nu}$ is linear in $h_{\mu\nu}$ and $R^{(2)}_{\mu\nu}$ is quadratic in $h_{\mu\nu}$. Now, we can look at the high frequency and low frequency limits. First, $\bar{R}_{\mu\nu}$ contains only terms

of $\bar{g}_{\mu\nu}$ and is therefore only of importance in the low frequency limit. Since $R^{(1)}_{\mu\nu}$ is linear in $h_{\mu\nu}$, it will only matter in the high frequency limit. Whereas, $R^{(2)}_{\mu\nu}$ is quadratic in $h_{\mu\nu}$ so it will play a part in both the high and low frequency limit [Mag08]. For now we will focus on the low frequency limit, giving us

$$\bar{R}_{\mu\nu} = -[R^{(2)}_{\mu\nu}]^{\text{Low}} + \frac{8\pi G}{c^4}(T_{\mu\nu} - \frac{1}{2}g_{\mu\nu}T)^{\text{Low}}. \tag{2.32}$$

Now let us introduce a time-scale $\bar{t}$ such that $\frac{1}{f} \ll \bar{t} \ll \frac{1}{f_B}$. During a time of $\bar{t}$, there fit many periods of the waves $\frac{1}{f}$, so these average out. Whereas the background does not change that much. This allows us to average over this time-scale $\bar{t}$. We will get

$$\bar{R}_{\mu\nu} = -\langle R^{(2)}_{\mu\nu}\rangle + \frac{8\pi G}{c^4}\langle T_{\mu\nu} - \frac{1}{2}g_{\mu\nu}T\rangle. \tag{2.33}$$

Where $\langle \dots \rangle$ denotes the average over $\bar{t}$. Next we will define the tensor $t_{\mu\nu}$ given by

$$t_{\mu\nu} = -\frac{c^4}{8\pi G}\langle R^{(2)}_{\mu\nu} - \frac{1}{2}g_{\mu\nu}R^{(2)}\rangle. \tag{2.34}$$

In this definition

$$R^{(2)} = \bar{g}^{\mu\nu}R^{(2)}_{\mu\nu}, \tag{2.35}$$

and its trace is

$$t = \bar{g}^{\mu\nu}t_{\mu\nu} = +\frac{8\pi G}{c^4}\langle R^{(2)}\rangle. \tag{2.36}$$

We can use these definitons to rewrite eq. (2.33) to

$$\bar{R}_{\mu\nu} - \frac{1}{2}\bar{g}_{\mu\nu}\bar{R} = \frac{8\pi G}{c^4}(\bar{T}_{\mu\nu} + t_{\mu\nu}). \tag{2.37}$$

We call this the "croase-grained" form of the Einstein equations. Here the effect that matter with an energy-momentum tensor $t_{\mu\nu}$ can be identified with the effect that gravitiational waves have on the background curvature.

Due to the averaging in $t_{\mu\nu}$, $R^{(2)}_{\mu\nu}$ can be simplified by integrating by parts, as well as neglecting boundary terms. It will then simplify to [Mag08]

$$t_{\mu\nu} = \frac{c^4}{32\pi G}\langle \partial_\mu h_{\alpha\beta}\partial_\nu h^{\alpha\beta}\rangle. \tag{2.38}$$

This expression is gauge-invariant, again because of averaging. Therefore, we can transpose it to the transverse traceless gauge to get

$$t^{00} = \frac{c^2}{32\pi G}\langle \dot{h}^{TT}_{ij}\dot{h}^{TT}_{ij}\rangle = \frac{c^2}{16\pi G}\langle \dot{h}^2_+ + \dot{h}^2_\times\rangle. \tag{2.39}$$

Finally, according to [Mag08] the energy caused by gravitational waves in a volume V with boundary surface S of radius r is

$$\frac{dE_V}{dt} = -c \int_S dA t^{00}. \tag{2.40}$$

So energy emitted in gravitational waves is

$$\frac{dE_{\mathrm{GW}}}{dt} = -\int_{\mathcal{V}} d^3x \, \partial_t t^{00}. \tag{2.41}$$

Now by writing a surface element as $dA = r^2 d\Omega$, we find the result

$$\frac{dE_{\mathrm{GW}}}{dt} = \frac{c^3 r^2}{16\pi G} \int d\Omega \langle \dot{h}_+^2 + \dot{h}_\times^2 \rangle. \tag{2.42}$$

2.5 Detection of gravitational waves

Before getting into data analysis, it is important to understand how gravitational waves are detected. First of all, because the perturbations in the field are so small, detecting a gravitational wave is extremely difficult. Due to this reason the first gravitational waves were only detected in 2015 at the LIGO stations in Hanford, Wahsington, Livingstone, Louisiana [BPA16]. Since then many different events were observed and detected, including the two events with big relative mass difference in 2019. There are five stations across the world that can meassure gravitational waves: The two LIGO stations in Livingstone and Hanford, Virgo in Cascina, Italy, Kagra in Kamioka, Hida, Japan, and finally GEO600 in Hannover, Germany. There is another LIGO detection station to be build in India in the next few years.

Gravitational waves disrupt the spacetime on earth. Space around us is either streched or sqeezed. This also influences traveling light. The detectors use this to measure differences in lengths between the arms of the detector. In figure 3 the process of detection is shown. From a laser source emerges a light beam of constant wavelength. This beam will be partially split by the beam-splitting mirror. Two separate beams will then travel through the two arms of the detector. These arms are called the x-arm and the y-arm of the dectector. The beams are then reflected back by a mirror and end up back at the beam-splitter. If there is no gravitational wave present, the two beams will be out of phase and there will be distructive interference. Consequently, no signal will reach the light detector. However, when there is a gravitational wave present, the length of the two arms will fluctuate. Therefore, the x-arm and y-arm will not have the same length and the two signals will not cancel each other out completely: a signal is detected. In order to be able to detect gravitational waves, the detectors must be sensitive to relative changes in length of $\frac{\Delta L}{L} < 10^{-21}$.

Now that we have an understanding of how the detectors work, we can look at how

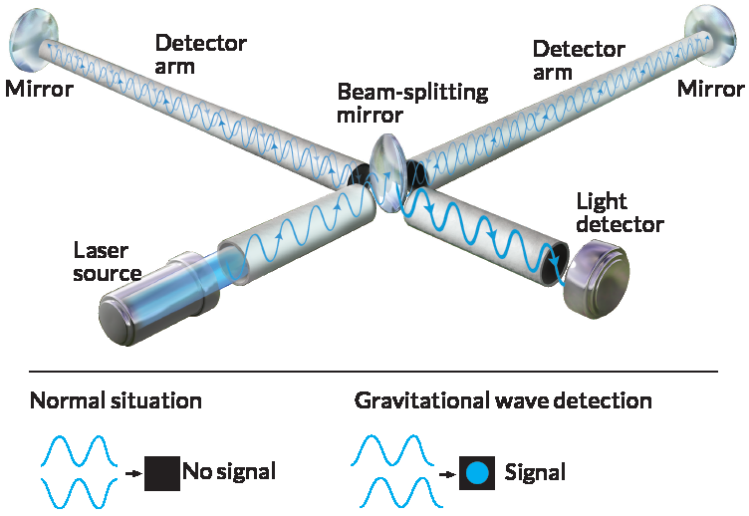

Figure 3: A sketch of a gravitational wave detector

we can interpret the detected signal and how this signal is related to the gravitational wave. In the perspective of the detector, we have a metric perturbation of

$$h_{ij} = \begin{pmatrix} h_{xx} & h_{xy} & h_{xz} \\ h_{yx} & h_{yy} & h_{yz} \\ h_{zx} & h_{zy} & h_{zz} \end{pmatrix}. \tag{2.43}$$

Our total metric is $g_{\mu\nu} = \eta_{\mu\nu} + h_{\mu\nu}$, or in other words $ds^2 = -c^2dt^2 + (\delta_{ij} + h_{ij})dx^i dx^j$. The light from the laser beam moves on a lightlike geodesics. Therefore, $ds^2 = 0$. Furthermore, in the x-arm light only moves in the x direction, so we can set $dy = dz = 0$. Our metric then becomes $c^2dt^2 = (1 + h_{xx})dx^2$. Likewise, for the light beam in the y-arm we have $c^2dt^2 = (1 + h_{yy})dy^2$. Then the time for the light to travel through the x-arm becomes

$$\Delta t_x = 2\int_{\text{BS}}^{\text{mirror}} dt \tag{2.44}$$

$$= \frac{2}{c}\int_{x_{\text{BS}}}^{x_{\text{mirror}}} (1 + h_{xx})^{\frac{1}{2}} dx \tag{2.45}$$

$$\approx \frac{2}{c}(x_{\text{mirror}} - x_{\text{BS}})(1 + h_{xx})^{\frac{1}{2}} \tag{2.46}$$

$$\approx (1 + \frac{1}{2}h_{xx})\frac{2L}{c}. \tag{2.47}$$

We can estimate h_{xx} to be constant over the x-arm to approximate the integral, because the period T of a gravitational wave is much larger then the travel time of the light through the arm $T = \frac{\lambda_{\text{GW}}}{c} \gg \frac{2L}{c}$ [Mag08]. Furthermore, since h_{xx} contains only small perturbations, we can use a Taylor expansion to estimate $(1+h_{xx})^{1/2}$ to $(1+\frac{1}{2}h_{xx})$. In the

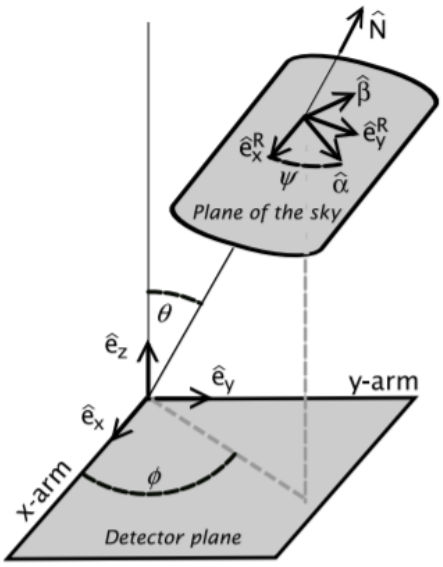

Figure 4: In this figure a sketch is given of how a binary black hole system may be orientated with respect to a detector on earth

same way we will find that $\Delta t_y \approx (1+\frac{1}{2}h_{yy})\frac{2L}{c}$. The interferometer senses the difference in travel time compared to the time it would take if no wave is present. So define $\Delta t_0 = \frac{2L}{c}$, then

$$h(t) = \frac{\Delta t_x - \Delta t_y}{\Delta t_0} = \frac{1}{2}(h_{xx} - h_{yy}). \tag{2.48}$$

In the previous subsection the Transpose Traceless gauge was introduced. This had been done to express the waveform in terms of h_+ and $h_\times$ in an easy and natural way. However, in this process we assumed that the observer is standing on the z-axis. This is of course not always the case, as can be seen in figure 4. We will have to make use of a rotation $\mathcal{R}$ given by

$$\mathcal{R} = \begin{pmatrix} \cos\varphi & \sin\varphi & 0 \\ -\sin\varphi & \cos\varphi & 0 \\ 0 & 0 & 1 \end{pmatrix} \begin{pmatrix} 1 & 0 & 0 \\ 0 & \cos\theta & -\sin\theta \\ 0 & \sin\theta & \cos\theta \end{pmatrix} \begin{pmatrix} \cos\psi & \sin\psi & 0 \\ -\sin\psi & \cos\psi & 0 \\ 0 & 0 & 1 \end{pmatrix}. \tag{2.49}$$

Then the transformation $h_{ij} = (\mathcal{R}h^{TT}\mathcal{R}^T)_{ij}$, will let us express the strain $h(t)$ in terms of h_+ and $h_\times$. This gives

$$h(t) = F_+(\varphi,\theta,\psi)h_+(t) + F_\times(\varphi,\theta,\psi)h_\times(t). \tag{2.50}$$

Where the beam patern functions are

$$F_+ = \frac{1}{2}(1+\cos^2(\theta))\cos(2\varphi)\cos(2\psi) - \cos(\theta)\sin(2\varphi)\sin(2\psi), \tag{2.51}$$

$$F_\times = \frac{1}{2}(1+\cos^2(\theta))\cos(2\varphi)\sin(2\psi) + \cos(\theta)\sin(2\varphi)\cos(2\psi). \tag{2.52}$$

3 Gravitational waves data analysis

When detecting gravitational waves signals we mostly get an enormous amount of data. In order to navigate through this bulk of data we have to make use of complex algorithms to filter out noise and identify signals. First we will make use of matched filtering. This is an algorithm that checks which precalculated signals matches best with the data. After which we will use nested sampling to check how reliable the match is.

3.1 Detection: Matched filtering, template banks

Data consists mostly of noise. However, there are tricks to look beyond the noise and dig out signals. A way to do this is with matched filtering. Matched filtering is an algorithm that finds the waveform that fits best with the data. It even works when some parameters, like the amplitude of the signal or the starting time, are unknown. In fact it can even determine the values of these parameters. Matched filtering works by integrating an expected waveform over the signal. It makes use of the fact that the noise is random and therefore becomes less important when integrating over a longer time. Matched filtering is the best known linear filter to extract a signal which is hidden in stationary Gaussian noise [Tur60].

Assume that we have a gravitational wave $h(t)$. Then the meassured strain $s(t)$ can be described by the sum of the signal plus the noise $s(t) = n(t) + h(t)$, where $n(t)$ resembles the noise. Lets say we more or less know the form of the signal $h(t)$. Then we can integrate $h(t)$ against $s(t)$ over the observation time T. this will give us

$$\frac{1}{T}\int_0^T s(t)h(t)dt = \frac{1}{T}\int_0^T n(t)h(t)dt + \frac{1}{T}\int_0^T h(t)^2 dt. \tag{3.1}$$

The last integral will be of the order h_0^2, where h_0 resembles the charateristic signal amplitude. Whereas the value of the first integral on the righthand side will be of the order $\frac{\sqrt{\tau_0}}{\sqrt{T}} n_0 h_0$. Here n_0 is the characteristic amplitude of the noise and τ_0 the typical period of the gravitational wave. This can be explained since the noise is random so the value of the integral will be like a random walk which takes the value $\frac{1}{\sqrt{T}} n_0 h_0$. However, the integral should be dimensionless. Therefore we have to multiply by another value which has dimension time. The only logical parameter would be τ_0. So the integral will be of this order.

This way of integrating has as a property that when $T \to \infty$ the noise contribution will dissapear. In fact the amplitude of the signal does not even have to be bigger than the amplitude of the noise. Since when $h_0 > \frac{\sqrt{\tau_0}}{\sqrt{T}} n_0$, we already have that the second integral will be dominant over the first. For example, with binary coalesence the typical period is $\tau_0 \approx 10^{-2} s$. Therefore, if we take $T = 100s$, we already have that $\frac{\sqrt{\tau_0}}{\sqrt{T}} \approx 10^{-2}$. Consequently, we can measure a signal with 100 times lower amplitude than the noise.

As explained in section 2 the detector data we have to deal with is a time series. If this would be only noise we would have that $(n(t_0), n(t_1), \ldots, n(t_N))$ where $t_{i+1} = t_i + \Delta t$. Often it is more convinient to work in the frequency domain. Therfore we take the discrete fourier transform and work with $(\tilde{n}(f_0), \tilde{n}(f_1), \ldots, \tilde{n}(f_N))$, where $f_{i+1} = f_i + \Delta f$. We will use the notation $\tilde{n}_i = \tilde{n}(f_i)$. Not all noise realizations have the same probability. Assume that the noise probability distribution $p(\tilde{n}_i)$ is Gaussian and stationary. So

$$p(\tilde{n}_i) \propto e^{-\frac{|\tilde{n}_i|^2}{2\sigma_i^2}}. \tag{3.2}$$

The probability density for noise realization as a whole will then be given by

$$p[n] = p(\tilde{n}_0, \tilde{n}_1, \ldots, \tilde{n}_N) = \prod_{i=0}^{N} \mathcal{N} e^{-\frac{|\tilde{n}_i|^2}{2\sigma_i^2}}. \tag{3.3}$$

We can change the product of the probabilities to a sum inside the exponent. Then we will take the continuum limit to find

$$p[n] = \mathcal{N} e^{-\int_{-\infty}^{\infty} \frac{|\tilde{n}(f)|^2}{S_n(f)} df}. \tag{3.4}$$

In this equation we defined $S_n(f) = \frac{1}{2}\sigma_i^2 \Delta f$. Instead of just integrating the waveform against the signal we will try and look for a more optimal filter $K(t)$. We define

$$\hat{s} = \int_{-\infty}^{\infty} s(t) K(t) dt. \tag{3.5}$$

Furthermore, we make two other definitions. Namely S which will be the expected value when a signal h is present. S is defined as $S = \langle \hat{s} \rangle_h$. The other definition we make is N which will be the root-mean-square value when no signal is present. N is given by $N = [\langle s^2 \rangle_{h=0} - \langle s \rangle_{h=0}^2]^{\frac{1}{2}}$. This will enable us to define the signal-to-noise ratio given by

$$S/N = \frac{\langle \hat{s} \rangle_h}{[\langle s^2 \rangle_{h=0} - \langle s \rangle_{h=0}^2]^{\frac{1}{2}}}. \tag{3.6}$$

Our goal is to find which $K(t)$ optimizes S/N. We will do this assuming there is a signal $h(t)$ present. First of all it is confenient to write S and N in the frequency domain. For S we have that

$$\begin{aligned} S &= \langle s \rangle_h && (3.7)\\ &= \int_{-\infty}^{\infty} \langle s(t) \rangle K(t) dt && (3.8)\\ &= \int_{-\infty}^{\infty} h(t) K(t) dt && (3.9)\\ &= \int_{-\infty}^{\infty} \tilde{h}(f) \tilde{K}^*(f) df. && (3.10) \end{aligned}$$

Likewise we can find for N that

$$N = [\langle s^2 \rangle_{h=0} - \langle s \rangle^2_{h=0}]^{\frac{1}{2}} \tag{3.11}$$

$$= \langle s^2 \rangle^{\frac{1}{2}}_{h=0} \tag{3.12}$$

$$= [\int_{-\infty}^{\infty} \int_{-\infty}^{\infty} \langle n(t) n(t') \rangle K(t) K(t') dt dt']^{\frac{1}{2}} \tag{3.13}$$

$$= [\int_{-\infty}^{\infty} \frac{1}{2} S_n(f) |\tilde{K}^*(f)|^2 df]^{\frac{1}{2}}. \tag{3.14}$$

In the last line we used that $\langle \tilde{n}(f) \tilde{n}(f') \rangle = \frac{1}{2} \delta(f - f') S_n(f)$. What remains to be done is to define an inner product between two functions. We call it the noise-weighted inner product and define it as

$$(A|B) = \mathcal{R} \int_{-\infty}^{\infty} df \frac{\tilde{A}^*(f) \tilde{B}(f)}{\frac{1}{2} S_n(f)} = 4\mathcal{R} \int_0^{\infty} \frac{\tilde{A}^*(f) \tilde{B}(f)}{S_n(f)}. \tag{3.15}$$

Now we can rewrite S/N to

$$S/N = \frac{(\mathbf{K}|h)}{\sqrt{(\mathbf{K}|\mathbf{K})}} = (\hat{\mathbf{K}}|h). \tag{3.16}$$

Where we defined $\mathbf{K} = \frac{1}{2} S_n(f)$ and $\hat{\mathbf{K}} = \frac{\mathbf{K}}{\sqrt{(\mathbf{K}|\mathbf{K})}}$. From eq. (3.16) we can see that to optimize the signal-to-noise ratio is we have to point $\mathbf{K}$ in the same direction as h. In other words, S/N is maximal when $\mathbf{K}(t) \propto h(t)$ or $\tilde{\mathbf{K}}(f) \propto \frac{\tilde{h}(f)}{S_n(f)}$.

In reality we have to match the signal with many different waveforms h_i. Therefore, we have to use many different filters $\hat{\mathbf{K}}_\mathbf{i} \propto h_i$. Furthermore, we do not know $\langle s \rangle$. We only know the actual value of s. Consequently we approximate the signal to noise ratio for a given trial waveform h_i by

$$\left(\frac{S}{N} \right)_i = \frac{(h_i|s)}{\sqrt{(h_i|h_i)}}. \tag{3.17}$$

In binary coalescences, the waveform is dependent on certain parameters $\bar{\theta} = (\theta_0, \theta_1, \ldots, \theta_N)$. We cannot evaluate the waveform over different values for these parameters in a continious fassion. Therefore, we have to lay out template banks over parameter space. Where a point $\bar{\theta}_i$ in the template bank gives a trial waveform $h_i = h(\bar{\theta}_i)$. To find the waveform that fits the signal best, we have to maximize the signal to noise ratio over all the points in the template bank.

$$\left(\frac{S}{N} \right)_{\max} = \max_i \frac{(h(\bar{\theta}_i)|s)}{\sqrt{(h(\bar{\theta}_i)|h(\bar{\theta}_i))}}. \tag{3.18}$$

This template bank is high dimensional space. Therefore, the amount of points living inside of it grows quickly when you want neighbouring points to be close to each other.

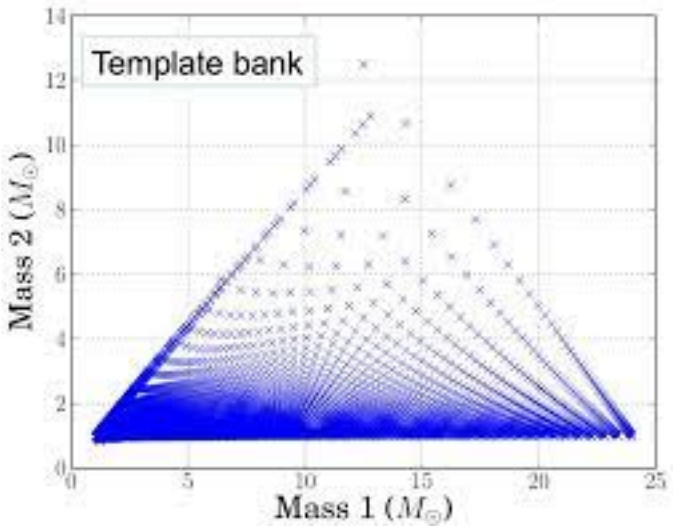

Figure 5: A template bank for the values of the masses of the black holes. Note that for higher masses the space between points becomes larger.

In order to make sure that we are not considering too many points we have to make use of the mismatch. To define the mismatch we first have to define the match between to neighbouring points. The match is given by

$$M = (\hat{h}(\bar{\theta})|\hat{h}(\bar{\theta} + \Delta\theta)). \tag{3.19}$$

Where $\hat{h} = \frac{h}{\sqrt{(h|h)}}$. Now if we expand this equation in small quantities of $\Delta\theta$, we find

$$M = (\hat{h}(\bar{\theta})|\hat{h}(\bar{\theta})) + \frac{\partial M}{\partial\theta^i}\Delta\theta^i + \frac{1}{2}\frac{\partial^2 M}{\partial\theta^i\partial\theta^j}\Delta\theta^i\Delta\theta^j = 1 + \frac{1}{2}\frac{\partial^2 M}{\partial\theta^i\partial\theta^j}\Delta\theta^i\Delta\theta^j. \tag{3.20}$$

Now we can define the quantity $g_{ij} = -\frac{1}{2}\frac{\partial^2 M}{\partial\theta^i\partial\theta^j}$. Then we can easily define the mismatch between neighbouring templates by

$$1 - M = g_{ij}\Delta\theta^i\Delta\theta^j. \tag{3.21}$$

In order to make sure that the spaces between neighbouring templates does not grow to large and to make sure we do not consider too many points, we can set the mismatch to a certain value. Then we make sure that the mismatch never out grows this value. An example of a template bank, only considering the values for the mass is shown in figure 5. Since g_{ij} becomes smaller for higher values of m_1 and m_2 there is more space between points in the template bank there.

3.2 Nested Sampling

In the previous subsection we saw how to check if a trial waveform fits the measured signal. Now we want to be certain that the set of parameter values that we find belongs

to the data. In other words, given the data d and the hypothesis $\mathcal{H}$, we want to know the probability that $\bar{\theta}$ contains the correct values for the parameters. In other words, we want to determine the posterior probability density, defined as $p(\bar{\theta}|d, \mathcal{H})$. Here $\mathcal{H}$ is not the explicit waveform but the hypothesis. For example, the hypothesis could be that the signal is created by the inspiral of two black holes. This would then bring a family of waveforms $h(\bar{\theta}, t)$. The data d is the detector data and is given by $d(t) = n(t) + h(\bar{\theta}, t)$. Using Bayes' theorem we can rewrite this probability to

$$p(\bar{\theta}|d, \mathcal{H}) = \frac{p(d|\mathcal{H}, \bar{\theta})p(\bar{\theta}|\mathcal{H})}{p(d|\mathcal{H})}. \tag{3.22}$$

Here $p(d|\mathcal{H}, \bar{\theta})$ is called the likelihood, $p(\bar{\theta}|\mathcal{H})$ is called the prior probability density and $p(d|\mathcal{H})$ is the evidence for the hypothesis. The prior probability density is something we can choose ourself. It should be based on what we know about the event before hand. The likelihood and the evidence is something that we are able to calculate.

First of all we calculate the likelihood. Note that the likelihood is the probability that we measure the data d given the hypothesis and the parameters. Since $d(t) = n(t) + h(\bar{\theta}, t)$ and since $h(\bar{\theta}, t)$ is given, this probability is equivalent to measuring a noise of $n(t) = d(t) - h(\bar{\theta}, t)$. To calculate the likelihood we will use eq. (3.4). Note that using the definition for the inner product between functions from eq. (3.15), eq. (3.4) can be rewritten to

$$p[n] = \mathcal{N} e^{-\frac{1}{2}(n|n)}. \tag{3.23}$$

Now we use that $d(t) = n(t) + h(\bar{\theta}, t)$ which means that $\tilde{n}(f) = \tilde{d}(f) - \tilde{h}(\bar{\theta}, f)$. Both h and d are known. Therefore, the above equation becomes

$$p[n] = \mathcal{N} e^{-\frac{1}{2}(d-h|d-h)}. \tag{3.24}$$

Now the only thing left is to calculate the evidence, then we have everything we need to calculate the posterior probability density. By multiplying both sides of eq. (3.22) by the evidence and then integrating over all θ_i we find that the evidence is equal to

$$p(d|\mathcal{H}) = \int \cdots \int p(d|\mathcal{H}, \bar{\theta})p(\bar{\theta}|\mathcal{H}) d\theta_1 \dots d\theta_N \tag{3.25}$$

$$= \int d^N\theta \, L(\bar{\theta})\pi(\bar{\theta}). \tag{3.26}$$

Here $L(\bar{\theta})$ resembles the likelihood and $\pi(\bar{\theta})$ the prior. As can be seen in eq. (3.25), to calculate the evidence we need to solve an integral of a high dimensionality. This can be done with the aid of nested sampling. Nested sampling transforms the above integral into an one dimensional integral making use of a scalar X called the prior mass. It depends on λ and it gives the fraction of prior mass volume with likelihood bigger then λ:

$$X(\lambda) = \int_{L(\bar{\theta})>\lambda} \pi(\bar{\theta}) d^N\theta. \tag{3.27}$$

The prior is normalized. Therefore, $X \in [0,1]$. A part of the posterior mass dX equals $\pi(\bar{\theta})d^N\theta$. Furthermore $X = 1$ is given by the integral over all the likelihood, so $\lambda = L_{\min}$. Likewise, $X = 0$ is given by the surface of maximum likelihood $\lambda = L_{\max}$. The evidence $Z = p(d|\mathcal{H})$ can be rewritten to

$$Z = \int \tilde{L}(X)dX. \tag{3.28}$$

The idea behind nested sampling is to find points θ_k corresponding to progressively higher likelihoods L_k, therefore decreasing X_k. This will let us approximate the evidence by

$$Z \approx \sum_k L_k \Delta X_k, \tag{3.29}$$

as well as the posterior density by

$$p(\bar{\theta}|d,\mathcal{H}) = \frac{L_k}{Z}\Delta X_k. \tag{3.30}$$

Nested sampling works by choosing M points in parameter space from the prior. These are called the live points. Each live point has a likelihood associated to it, and therefore a prior mass. First of all, we choose the point with the lowest likelihood L_0 and highest prior mass X_0 and replace it with a point with higher likelihood. Now a different point has lowest likelihood L_1 and highest prior mass X_1. Then repeat the previous step.

Since it is difficult to determine the prior mass X_k belonging to a point $\bar{\theta}_k$, the only way to get the prior mass is to approximate it with the aid of a probability distribution. The probability that all M points have a prior mass lower then $X = \chi$ is given by

$$P(X_i < \chi) = \prod_{i=1}^{M} \int_0^{\chi} dX_i = \prod_{i=1}^{M} \chi = \chi^M. \tag{3.31}$$

Therefore, the probability density that the maximum prior mass is at χ equals

$$p(\chi, M) = M\chi^{M-1}. \tag{3.32}$$

Now, we define the ratio between the old and new prior mass $t = \frac{X_1}{X_0}$. Then t has the same distribution as χ. Therefore we draw the shrinkage ratio from the distibution given in eq. (3.32). Which leads to

$$X_k = \prod_{i=1}^{k} t_i. \tag{3.33}$$

We will terminate the algorithm by comparing the amount of evidence that is still to be calculated with the amount of evidence we already have. The algorithm will terminate when

$$L_{\max,\text{cur}} X_{\text{cur}} < \alpha Z_{\text{cur}}, \tag{3.34}$$

where $L_{\max,\text{cur}}$ is the current maximum likelihood over all the points, X_{cur} is the current estimated prior mass, α is a constant to be chosen by the user and Z_{cur} is the current value for the evidence.

```
H = highest(Points)

while(H*X_new >= alpha*Z):
    p = lowest(Points)
    L = F(Points[p][0], Points[p][1])
    X_old = X_new
    X_new *= distribution()
    Z += L*(X_old - X_new)
    Posterior.append([Points[p][0], Points[p][1], L*( X_old - X_new)])
    replace(p, L, Points)
    newL = F(Points[p][0], Points[p][1])
    if newL > H:
        H = newL
```

Figure 6: Nested sampling algorithm implemented in python

3.3 Nested sampling in practice

Now we will look at an example to see how nested sampling works in practice. We consider the following function over two variables, where $x, y \in [-0.5, 0.5]$

$$F(x,y) = \frac{1}{2\pi\sigma_x\sigma_y} \exp\left[-\frac{x^2}{2\sigma_x^2} - \frac{y^2}{2\sigma_y^2}\right]. \tag{3.35}$$

We will set $\sigma_x = 0.1$ and $\sigma_y = 0.5$. Furthermore, we will use nested sampling to calculate

$$\int_{-0.5}^{0.5}\int_{-0.5}^{0.5} F(x,y)dxdy. \tag{3.36}$$

To determine this integral we will take the prior to be uniform over $[-0.5, 0.5]^2$. Therefore, the likelihood function will be equal to $F(x, y)$. We will consider 1000 points at the time and we set the termination constant $\alpha = \frac{1}{10000}$. In figure 6 we see the nested sampling algorithm implemented in python that is used to solve the integral. In this program the function highest(Points) returns the highest likelihood of all the current lived points. The function lowest(Points) returns the point with lowest likelihood of the lived points. The function distribution() returns a value drawn from the probability density given in eq. (3.32). To do this we have to define a primitive of eq. (3.32), this is given in eq. (3.31). Then find the inverse of this function, in this case $d(x) = x^{1/1000}$. Finally, we choose a random number x from the uniform distribution from 0 to 1 and fill that number into $d(x)$.

In the end Z will be an approximation of the evidence, in this case of the integral in eq. (3.36). Additionally, the array posterior will approximate the posterior as in eq. (3.30). The actual solution of the integral in eq. (3.36) is 0.682, this algorithm gives as an approximation 0.672, which is close enough. In figure 7 we see the approximated values of the posterior of the live points. Note that points cluster more at higher values of the likelihood, in our case $F(x, y)$, and are more spread for lower values.

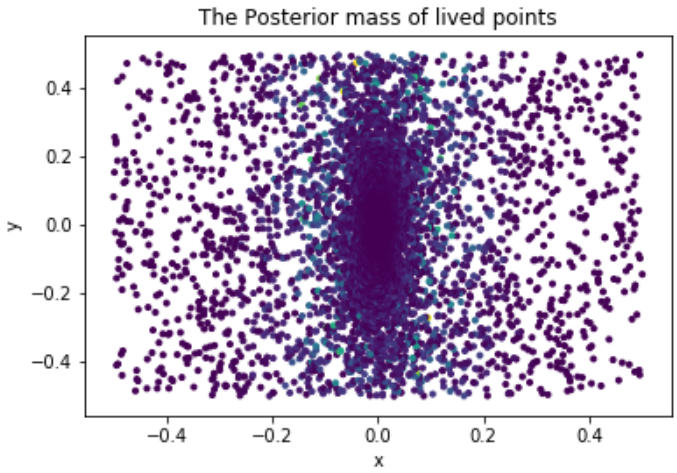

Figure 7: Posterior of lived points after the nested sampling algorithm has finished

4 Pertubative solutions to the linearized Einstein equations

In section 2 we have calculated the transverse traceless waveform h_{ij}^{TT} given a stress-energy tensor T_{kl}. In this section we will continue with this expression and find the solution for our specific problem, the merging of binary black holes. We will expand the expression up to 0.5 post Newtonian order. Finally we will take the fourier transform of the wave to express the wave in the fourier domain by

$$\tilde{h}(f,\theta,\varphi) = \sum_{l=2}^{\infty}\sum_{m=-l}^{l} \tilde{h}^{lm}(f)\,{}_{-2}Y^{lm}(\theta,\varphi). \tag{4.1}$$

4.1 Multipole expansion of the general solution

The transpose traceless form of the wave equation has the following expression

$$h_{ij}^{TT}(t,\mathbf{x}) = \frac{4G}{c^4}\Lambda_{ij,kl}(\hat{n})\int_{\mathcal{V}} d^3x' \frac{T^{kl}(t-\frac{|\mathbf{x}-\mathbf{x}'|}{c},\mathbf{x}')}{|\mathbf{x}-\mathbf{x}'|}. \tag{4.2}$$

Finding the exact solution to this integral is difficult. However, we can use a Taylor approximation to simplify the expression inside the integral. Since the inspiraling black holes will be far away of the observer, the size of the source will be much smaller than the distance between the observer and the source. In other words $|\mathbf{x}| \ll |\mathbf{x}'|$. This allows us to use the following simplification

$$|\mathbf{x}-\mathbf{x}'| = r - \mathbf{x}'\cdot\hat{n} + O\left(\frac{d^2}{r}\right). \tag{4.3}$$

Where $r = |\mathbf{x}|$. If we substitute this into the energy-momentum distribution T^{kl} and Taylor it. We will find that

$$T^{kl}(t-\frac{r-\mathbf{x}'\cdot\hat{n}}{c},\mathbf{x}') \approx T^{kl}(t-\frac{r}{c},\mathbf{x}')+\frac{x'^m\hat{n}^m}{c}\partial_t T^{kl}(t-\frac{r}{c},\mathbf{x}')+\frac{x'^m x'^n\hat{n}^m\hat{n}^n}{2c^2}\partial_t^2 T^{kl}(t-\frac{r}{c},\mathbf{x}')+\dots. \tag{4.4}$$

We can substitute 4.4 back into the integral of 4.2 to get the following expression

$$h_{ij}^{TT}(t,\mathbf{x}) = \frac{1}{r}\frac{4G}{c^4}\Lambda_{ij,kl}(\hat{n})\int_{\mathcal{V}} d^3\mathbf{x}' T^{kl}(t-\frac{r}{c},\mathbf{x}')+\frac{x'^m\hat{n}^m}{c}\partial_t T^{kl}(t-\frac{r}{c},\mathbf{x}')+\frac{x'^m x'^n\hat{n}^m\hat{n}^n}{2c^2}\partial_t^2 T^{kl}(t-\frac{r}{c},\mathbf{x}')+\dots. \tag{4.5}$$

Note that $\frac{1}{r-\mathbf{x}'\cdot\hat{n}}$ simplifies to $\frac{1}{r}$ if we assume that $|x'| \ll r$. This expression looks messier than 4.2 which we started with, but let us define momentum multipoles to make it more clear. We define the multipole moments in the following way

$$S^{kl,i_1\dots i_n}(t) = \int_{\mathcal{V}} d^3\mathbf{x} T^{kl}(t,\mathbf{x}) x^{i_1}\dots x^{i_n}. \tag{4.6}$$

Now we can express h_{ij}^{TT} in terms of multipole moments. We will get

$$h_{ij}^{TT}(t,\mathbf{x}) = \frac{1}{r}\frac{4G}{c^4}\Lambda_{ij,kl}(\hat{n})\left[S^{kl} + \frac{1}{c}n_m\dot{S}^{kl,m} + \frac{1}{2c^2}n_m n_p\ddot{S}^{kl,mp} + \dots\right]_{\text{ret}}. \tag{4.7}$$

Here ret stands for retarded time, meaning $t_{\text{ret}} = t - \frac{r}{c}$. It turns out that the multipole moments are still challenging to calculate. It will be useful to express them in terms of mass and momentum multipoles, of which the value can be determined more easily. We will first define what the mass and momentum multipoles are. The mass multipoles are defined by

$$M^{i_1\dots i_n} = \frac{1}{c^2}\int_{\mathcal{V}} d^3\mathbf{x}T^{00}(t,\mathbf{x})x^{i_1}\dots x^{i_n}. \tag{4.8}$$

And the momentum multipoles by

$$P^{k,i_1\dots i_n} = \frac{1}{c}\int_{\mathcal{V}} d^3\mathbf{x}T^{0k}(t,\mathbf{x})x^{i_1}\dots x^{i_n}. \tag{4.9}$$

We call M the mass monopole moment, M^i the mass dipole moment, M^{ij} the mass quadrupole moment, M^{ijk} the mass octupole moment, etc. This is equivalent for the momentum mulitpoles. Note that the mass multipoles are symmetric in all their indices, whereas the momentum multipoles are symmetric in all indices except for the first one. We can rewrite the quadrupole moment in terms of the mass quadrupole in the following way.

$$\begin{aligned} S^{kl} &= \int_{\mathcal{V}} d^3\mathbf{x}T^{kl}(t,\mathbf{x}) \\ &= \int_{\mathcal{V}} d^3\mathbf{x}T^{il}(t,\mathbf{x})\delta_i^k \\ &= \int_{\mathcal{V}} d^3\mathbf{x}T^{il}(t,\mathbf{x})\partial_i x^k. \end{aligned} \tag{4.10}$$

Then using integration by parts and the fact that $T^{kl} = 0$ on the border of $\mathcal{V}$ we find that

$$S^{kl} = -\int_{\mathcal{V}} d^3\mathbf{x}\partial_i T^{il}(t,\mathbf{x})x^k. \tag{4.11}$$

Now we can use conservation of energy-momentum to derive that $\partial_i T^{ik} = -\partial_0 T^{0k}$. This give us

$$\begin{aligned} S^{kl} &= \int_{\mathcal{V}} d^3\mathbf{x}\partial_0 T^{0l}(t,\mathbf{x})x^k \\ &= \int_{\mathcal{V}} d^3\mathbf{x}\partial_0 T^{0j}(t,\mathbf{x})x^k\partial_j x^l \qquad (4.12) \\ &= -\int_{\mathcal{V}} d^3\mathbf{x}\partial_j\partial_0 T^{0j}(t,\mathbf{x})x^k x^l - \int_{\mathcal{V}} d^3\mathbf{x}\partial_0 T^{0j}(t,\mathbf{x})\partial_j x^k x^l. \qquad (4.13) \end{aligned}$$

Note that the second integral of line 4.13 is the same as the integral in line 4.12 just with k and l reversed. However S^{kl} is symmetric so the second integral in line 4.13 is just S^{kl}. Therefore, this becomes

$$\begin{aligned} S^{kl} &= \int_{\mathcal{V}} d^3\mathbf{x}\partial_0^2 T^{00}(t,\mathbf{x})x^k x^l - S^{kl} \\ &= \frac{1}{c^2}\int_{\mathcal{V}} d^3\mathbf{x}\ddot{T}^{00}(t,\mathbf{x})x^k x^l - S^{kl} \\ &= \ddot{M}^{kl} - S^{kl}. \end{aligned} \tag{4.14}$$

We conclude that

$$S^{kl} = \frac{1}{2}\ddot{M}^{kl}. \tag{4.15}$$

Now we have proven it for the quadrupole moment, we will try to find a relation between the octupole moment and the mass octupole and momentum octupole. We can express the octupole moment in terms of the momentum octupoles by

$$S^{ij,k} = \frac{1}{2}(\dot{P}^{i,jk} - \dot{P}^{k,ij} + \dot{P}^{j,ik}). \tag{4.16}$$

By looking at the integral of $S^{ij,k}$ and use the same trick from the previous lemma and integration by parts we will quickly see that

$$\begin{aligned} S^{ij,k} &= \int_{\mathcal{V}} d^3\mathbf{x}T^{ij}(t,\mathbf{x})x^k \\ &= \int_{\mathcal{V}} d^3\mathbf{x}T^{il}(t,\mathbf{x})x^k\partial_l x^j \\ &= \int_{\mathcal{V}} d^3\mathbf{x}\partial_0 T^{i0}(t,\mathbf{x})x^k x^j - \int_{\mathcal{V}} d^3\mathbf{x}T^{ik}(t,\mathbf{x})x^j \\ &= \dot{P}^{i,jk} - S^{ik,j}. \end{aligned} \tag{4.17}$$

Then by renaming the indices and using the fact that $S^{ij,k}$ is symmetric in the first two indices, we also find that

$$S^{ik,j} = \dot{P}^{k,ij} - S^{jk,i}, \tag{4.18}$$

$$S^{jk,i} = \dot{P}^{j,ik} - S^{ij,k}. \tag{4.19}$$

Then by consequently substituting eq. (4.18) in eq. (4.17) and then also substituting eq. (4.19) in the remaining expression we end up with

$$S^{ij,k} = \dot{P}^{i,jk} - \dot{P}^{k,ij} + \dot{P}^{j,ik} - S^{ij,k}. \tag{4.20}$$

Which we can rewrite to equation (4.16).

Next we will look at the relation between the momentum octupole moment and the mass octupole moment. The relation between the momentum octupole moment and mass octupole moment is given by

$$\ddot{M}^{ijk} = \dot{P}^{i,jk} + \dot{P}^{j,ik} + \dot{P}^{k,ij}. \tag{4.21}$$

We will again use the same trick with integration by parts. We start with writing out the integral.

$$\begin{aligned}
\dot{P}^{i,jk} &= \int d\mathbf{x}^3 \partial_0 T^{0i} x^j x^k \\
&= \int d\mathbf{x}^3 \partial_0 T^{0l} x^j x^k \partial_l x^i \\
&= -\int d\mathbf{x}^3 \partial_l \partial_0 T^{0l} x^i x^j x^k - \int d\mathbf{x}^3 \partial_0 T^{0l} x^i \partial_l x^j x^k - \int d\mathbf{x}^3 \partial_0 T^{0l} x^i x^j \partial_l x^k \\
&= \int d\mathbf{x}^3 (\partial_0)^2 T^{00} x^i x^j x^k - \int d\mathbf{x}^3 \partial_0 T^{0j} x^i x^k - \int d\mathbf{x}^3 \partial_0 T^{0k} x^i x^j \\
&= \ddot{M}^{ijk} - \dot{P}^{j,ik} - \dot{P}^{k,ij}.
\end{aligned} \tag{4.22}$$

We can rewrite this to eq. (4.21). Finally, we can easily combine eq. (4.16) and eq. (4.21) to find the final result

$$S^{ij,k} = \frac{1}{2}\ddot{M}^{ijk} - \dot{P}^{k,ij}. \tag{4.23}$$

To conclude, the quadrupole moment and the octupole moment can be expressed in terms of the mass quadrupole and mass and momentum octuopole. Therefore the waveform from eq. (4.7) can be rewritten in terms of the multipoles, using eq. (4.16) and (4.15). The result becomes

$$h_{ij}^{TT}(t, \mathbf{x}) = \frac{1}{r}\frac{4G}{c^4}\Lambda_{ij,kl}(\hat{n}) \left[\frac{1}{2}\ddot{M}^{kl} + \frac{1}{c}n_m\left(\frac{1}{2}\dddot{M}^{klm} - \ddot{P}^{m,kl}\right)\right]_{\text{ret}}. \tag{4.24}$$

4.2 Binary inspiral

The inspiral is the first step in the process of merging black holes. The black holes move in a gradually shrinking orbit. Due to the shrinkage of the radius, gravitational waves are being emitted by the black holes. As the black holes get closer to each other their speed increases. They will keep on spiraling, and as they get closer to each other the orbit shrinks even quicker, until they reach the last stable orbit or innermost circular stable orbit (ISCO). After this the merger will take place.

To describe the inspiraling black holes movement we will use their center of mass as an origin. We define the following quantities: let m_1 and m_2 be the mass of the two black holes respectively and $M = m_1 + m_2$ the total mass of the system. Additionally, we define $\mu = \frac{m_1 m_2}{M}$ as the reduced mass. Furthermore, if the first black hole is positioned at $\mathbf{x}_1(t)$

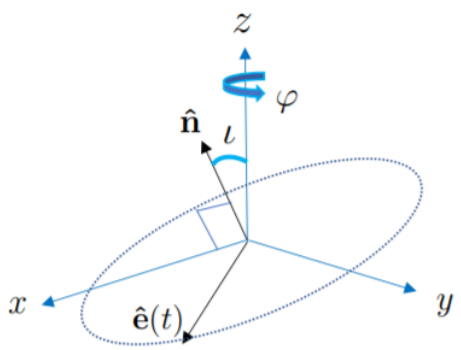

Figure 8: The angles φ and ι that the movement of the binaries depend on.

and the second black hole at $\mathbf{x}_2(t)$, then we define the distance between the two black holes as $R = |\mathbf{x}_1 - \mathbf{x}_2|$. Finally, we define $\hat{\mathbf{e}}(t)$ as the vector pointing from black hole 1 to black hole 2. Therefore

$$\mathbf{x}_1(t) - \mathbf{x}_2(t) = R\hat{\mathbf{e}}(t) \tag{4.25}$$

Using the fact that the origin is at the center of mass we know that

$$\frac{1}{M}(m_1\mathbf{x}_1(t) + m_2\mathbf{x}_2(t)) = 0 \tag{4.26}$$

We can use eq. (4.25) to find the relations

$$\mathbf{x}_1(t) = \frac{m_2}{M}R\hat{\mathbf{e}}(t) = \frac{\mu}{m_1}R\hat{\mathbf{e}}(t) \tag{4.27}$$

$$\mathbf{x}_2(t) = -\frac{m_1}{M}R\hat{\mathbf{e}}(t) = -\frac{\mu}{m_2}R\hat{\mathbf{e}}(t) \tag{4.28}$$

As one can see in the sketch in figure 8 the position of the binary system is dependent on two angles ι and φ. Here ι is called the inclination angle and can be between 0 and π. On the other hand, φ gives the starting position at $t = 0$ with respect to the x, y-plane. Note that ι just rotates the spiral around the x-axis, and φ is just a shift in phase for the binary. It will later turn out to be useful to define the starting position for $\varphi = 0$ and $\iota = 0$ at $\hat{\mathbf{e}}(0) = (cos(\pi/2), sin(\pi/2), 0)$. Therefore, we can describe the inspiral by

$$\hat{\mathbf{e}}(t) = \begin{pmatrix} 0 & 0 & 0 \\ 0 & \cos\iota & -\sin\iota \\ 0 & \sin\iota & \cos\iota \end{pmatrix} \begin{pmatrix} \cos(\omega t + \frac{\pi}{2} - \varphi) \\ \sin(\omega t + \frac{\pi}{2} - \varphi) \\ 0 \end{pmatrix} = \begin{pmatrix} -\sin(\omega t)\cos\varphi + \cos(\omega t)\sin\varphi \\ \cos\iota\cos(\omega t)\cos\varphi + \cos\iota\sin(\omega t)\sin\varphi \\ \sin\iota\cos(\omega t)\cos\varphi + \sin\iota\sin(\omega t)\sin\varphi \end{pmatrix}. \tag{4.29}$$

Here ω is expressed as a constant which represents the angular frequency of the spiraling black holes. As explained in the begining of the subsection this is in fact not a constant, but changes as the black holes get closer to each other. We can describe this change using the stationary phase approximation. We will do this in subsection 4.5.

4.3 Harmonics of the gravitational wave signal

To get the actual expression of the waveform h_{ij}^{TT}, we first have to solve the integrals of $\ddot{M}^{kl}$, $\dddot{M}^{kl,m}$ and $\ddot{P}^{m,kl}$. We will use the equation of motion given in eq. (4.27) and eq. (4.28), where $\hat{\mathbf{e}}(t)$ is given by eq. (4.29). For the integral of M^{kl} this will give

$$M^{kl} = \frac{1}{c^2}\int d\mathbf{x}'^3 T^{00} x'^k x'^l. \tag{4.30}$$

$T^{00}(t, \mathbf{x}')$ is given by $c^2\rho(t, \mathbf{x}')$. In our case we approximate the density of the black holes to where all the mass is in their center. Therefore,

$$\rho(t, \mathbf{x}') = m_1\delta^3(\mathbf{x}_1(t) - \mathbf{x}') + m_2\delta^3(\mathbf{x}_2(t) - \mathbf{x}'). \tag{4.31}$$

We get

$$\begin{aligned} M^{kl} &= \int d^3\mathbf{x}'(m_1\delta^3(\mathbf{x}_1(t) - \mathbf{x}' + m_2\delta^3(\mathbf{x}_2(t) - \mathbf{x}'))x'^k x'^l \\ &= m_1 x_1^k(t)x_1^l(t) + m_2 x_2^k(t)x_2^l(t) \\ &= m_1\left(\frac{\mu}{m_1}R\hat{e}^k(t)\right)\left(\frac{\mu}{m_1}R\hat{e}^l(t)\right) + m_2\left(\frac{\mu}{m_2}R\hat{e}^k(t)\right)\left(\frac{\mu}{m_2}R\hat{e}^l(t)\right) \\ &= \mu R^2\hat{e}^k(t)\hat{e}^l(t). \end{aligned} \tag{4.32}$$

Likewise, for $M^{kl,m}$ we find

$$\begin{aligned} M^{klm} &= \frac{1}{c^2}\int d^3\mathbf{x}' T^{00} x'^k x'^l x'^m \\ &= \int d^3\mathbf{x}'(m_1\delta^3(\mathbf{x}_1(t) - \mathbf{x}' + m_2\delta^3(\mathbf{x}_2(t) - \mathbf{x}'))x'^k x'^l x'^m \\ &= m_1 x_1^k(t)x_1^l(t)x_1^m(t) + m_2 x_2^k(t)x_2^l(t)x_2^m(t) \\ &= m_1\left(\frac{\mu}{m_1}R\hat{e}^k(t)\right)\left(\frac{\mu}{m_1}R\hat{e}^l(t)\right)\left(\frac{\mu}{m_1}R\hat{e}^m(t)\right) \\ &+ m_2\left(\frac{\mu}{m_2}R\hat{e}^k(t)\right)\left(\frac{\mu}{m_2}R\hat{e}^l(t)\right)\left(\frac{\mu}{m_2}R\hat{e}^m(t)\right) \\ &= \frac{m_2 - m_1}{M}\mu R^3\hat{e}^k(t)\hat{e}^l(t)\hat{e}^m(t). \end{aligned} \tag{4.33}$$

For $P^{m,kl}$ we will need an expression for T^{0m}. It is given by

$$T^{0m} = c(m_1 v_1^m\delta^3(\mathbf{x}_1(t) - \mathbf{x}') + m_2 v_2^m\delta^3(\mathbf{x}_2(t) - \mathbf{x}')). \tag{4.34}$$

Consequently the integral becomes

$$\begin{aligned}
P^{m,kl} &= \frac{1}{c}\int d^3\mathbf{x}' T^{0i}(t,\mathbf{x}) x'^k x'^l \\
&= \int d^3\mathbf{x}' m_1 v_1^m \delta^3(\mathbf{x}_1(t)-\mathbf{x}') + m_2 v_2^m \delta^3(\mathbf{x}_2(t)-\mathbf{x}') x'^k x'^l \\
&= m_1 v_1^m(t) x_1^k(t) x_1^l(t) + m_2 v_2^m(t) x_2^k(t) x_2^l(t) \\
&= m_1 \left(\frac{\mu}{m_1} R\hat{e}^k(t)\right)\left(\frac{\mu}{m_1} R\hat{e}^l(t)\right)\left(\frac{\mu}{m_1} R\dot{\hat{e}}^m(t)\right) \\
&+ m_2 \left(\frac{\mu}{m_2} R\hat{e}^k(t)\right)\left(\frac{\mu}{m_2} R\hat{e}^l(t)\right)\left(\frac{\mu}{m_2} R\dot{\hat{e}}^m(t)\right) \\
&= \frac{m_2-m_1}{M}\mu R^3 \hat{e}^k(t)\hat{e}^l(t)\dot{\hat{e}}^m(t). \qquad (4.35)
\end{aligned}$$

We will assume that the observer of the gravitational wave is located on the z-axis. Taking $\hat{n}=\hat{z}$ will change eq. (4.24) to

$$h_{ij}^{TT}(t,\mathbf{x}) = \frac{1}{r}\frac{4G}{c^4}\Lambda_{ij;kl}(\hat{z})\left[\frac{1}{2}\ddot{M}^{kl} + \frac{1}{c}\left(\frac{1}{2}\dddot{M}^{kl3} - \ddot{P}^{3,kl}\right)\right]_{\text{ret}}. \qquad (4.36)$$

Now we will show that for any tensor A^{kl} the transverse traceless projection in the $\hat{z}$ direction is given by:

$$\Lambda_{ij;kl}(\hat{z})A^{kl} = \begin{pmatrix} \frac{A^{11}-A^{22}}{2} & A^{12} & 0 \\ A^{12} & -\frac{A^{11}-A^{22}}{2} & 0 \\ 0 & 0 & 0 \end{pmatrix} \qquad (4.37)$$

The transverse traceless projector is defined by $\Lambda_{ij;kl}(\hat{n}) = P_{ik}P_{jl} - \frac{1}{2}P_{ij}P_{kl}$, where $P_{ij} = \delta_{ij} - n_i n_j$. Therefore, if $\hat{n}=\hat{z}$, then $n_1 = n_2 = 0$ and $n_3 = 1$. So $P_{11} = P_{22} = 1$ and for all other combinations of i and j we have that $P_{ij} = 0$. So we have

$$\Lambda_{11;kl}A^{kl} = (P_{1k}P_{1l} - \frac{1}{2}P_{11}P_{kl})A^{kl} = A^{11} - \frac{1}{2}(A^{11}+A^{22}) = \frac{A^{11}-A^{22}}{2}, \qquad (4.38)$$

$$\Lambda_{12;kl}A^{kl} = (P_{1k}P_{2l} - \frac{1}{2}P_{12}P_{kl})A^{kl} = A^{12}, \qquad (4.39)$$

$$\Lambda_{i3;kl}A^{kl} = (P_{ik}P_{3l} - \frac{1}{2}P_{i3}P_{kl})A^{kl} = 0. \qquad (4.40)$$

Since $\Lambda_{ij;kl}(\hat{z})A^{kl}$ is traceless and symmetric by definition, we now have the value for all entries and we can see that eq. (4.37) is indeed correct. In section 2 we saw how h_{ij}^{TT} was defined in terms of h_+ and $h_\times$. Combining eq. (4.24) and eq. (4.37) we derive them as

$$h_+ = \frac{1}{r}\frac{4G}{c^4}\left[\frac{\ddot{M}^{11}-\ddot{M}^{22}}{4} + \frac{\dddot{M}^{113}-\dddot{M}^{223}}{4c} - \frac{\ddot{P}^{3,11}-\ddot{P}^{3,22}}{2c}\right], \qquad (4.41)$$

$$h_\times = \frac{1}{r}\frac{4G}{c^4}\left[\frac{1}{2}\ddot{M}^{12} + \frac{1}{c}\left(\frac{1}{2}\dddot{M}^{123} - \ddot{P}^{3,12}\right)\right]. \qquad (4.42)$$

Now we have the expressions for the integrals, as well as for the motion of the black holes we can combine them. In eq. (4.41) and eq. (4.42) we see exactly which multipole moments we need. We will find for the mass quadrupole moment that

$$\ddot{M}_{11} = 2\mu R^2\omega^2 \left[\cos(2\varphi)\cos(2\omega t) + \sin(2\varphi)\sin(2\omega t)\right], \tag{4.43}$$

$$\ddot{M}_{12} = 2\mu R^2\omega^2 \cos\iota \left[\cos(2\varphi)\sin(2\omega t) - \sin(2\varphi)\cos(2\omega t)\right], \tag{4.44}$$

$$\ddot{M}_{22} = -2\mu R^2\omega^2 \cos^2\iota \left[\cos(2\varphi)\cos(2\omega t) + \sin(2\varphi)\sin(2\omega t)\right]. \tag{4.45}$$

$$\tag{4.46}$$

For the mass octupole moment we find

$$\begin{aligned}\dddot{M}_{113} = \frac{\delta\mu R^3\omega^3}{4}\sin\iota[&\cos(\varphi)\sin(\omega t) - 27\cos(3\varphi)\sin(3\omega t)\\ &- \sin(\varphi)\cos(\omega t) + 27\sin(3\varphi)\cos(3\omega t)],\end{aligned} \tag{4.47}$$

$$\begin{aligned}\dddot{M}_{123} = \frac{\delta\mu R^3\omega^3}{4}\sin\iota\cos\iota[&\cos(\varphi)\cos(\omega t) + 27\cos(3\varphi)\cos(3\omega t)\\ &+ \sin(\varphi)\sin(\omega t) + 27\sin(3\varphi)\sin(3\omega t)],\end{aligned} \tag{4.48}$$

$$\begin{aligned}\dddot{M}_{223} = \frac{\delta\mu R^3\omega^3}{4}\sin\iota\cos^2\iota[&3\cos(\varphi)\sin(\omega t) + 27\cos(3\varphi)\sin(3\omega t)\\ &- 3\sin(\varphi)\cos(\omega t) - 27\sin(3\varphi)\cos(3\omega t)].\end{aligned} \tag{4.49}$$

Here $\delta = \frac{m_1 - m_2}{M}$. Finally, for the momentum octupole moment we have

$$\begin{aligned}\ddot{P}_{3,11} = \frac{\delta\mu R^3\omega^3}{4}\sin\iota[&3\cos(\varphi)\sin(\omega t) - 9\cos(3\varphi)\sin(3\omega t)\\ &- 3\sin(\varphi)\cos(\omega t) + 9\sin(3\varphi)\cos(3\omega t)],\end{aligned} \tag{4.50}$$

$$\begin{aligned}\ddot{P}_{3,12} = \frac{\delta\mu R^3\omega^3}{4}\sin\iota\cos\iota[&-\cos(\varphi)\cos(\omega t) + 9\cos(3\varphi)\cos(3\omega t)\\ &- \sin(\varphi)\sin(\omega t) + 9\sin(3\varphi)\sin(3\omega t)],\end{aligned} \tag{4.51}$$

$$\begin{aligned}\ddot{P}_{3,22} = \frac{\delta\mu R^3\omega^3}{4}\sin\iota\cos^2\iota[&\cos(\varphi)\sin(\omega t) + 9\cos(3\varphi)\sin(3\omega t)\\ &- \sin(\varphi)\cos(\omega t) - 9\sin(3\varphi)\cos(3\omega t)].\end{aligned} \tag{4.52}$$

Now we can fill these expressions into eq. (4.41) and eq. (4.42). If we use Kepler's third law and rewrite $R\omega = (GM\omega)^{\frac{1}{3}}$ and define $x = \left(\frac{GM\omega}{c^3}\right)^{\frac{2}{3}}$, then we find that

$$\begin{aligned} h_+ = \frac{2G\mu}{rc^2}x\big[&(1+\cos^2)\iota[-\cos(2\varphi)\cos(2\omega t) - \sin(2\varphi)\sin(2\omega t)] \\ &+ \frac{\delta}{32}x^{\frac{1}{2}}[\{21\sin\iota + \sin(3\iota)\}(\cos\varphi\cos(\omega t) + \sin\varphi\sin(\omega t)) \\ &+ \{45\sin\iota + 9\sin(3\iota)\}(-\cos(3\varphi)\cos(3\omega t) - \sin(3\varphi)\sin(3\omega t))]\big], \end{aligned} \tag{4.53}$$

$$\begin{aligned} h_\times = \frac{2G\mu}{rc^2}x\big[&-2\cos\iota[\cos(2\varphi)\sin(2\omega t) - \sin(2\varphi)\cos(2\omega t)] \\ &+ \frac{\delta}{4}x^{\frac{1}{2}}\cos\iota\sin\iota\{3(-\sin\varphi\cos(\omega t) + \cos\varphi\sin(\omega t)) \\ &+ 9(\sin(3\varphi)\cos(3\omega t) - \cos(3\varphi)\sin(3\omega t))\}\big]. \end{aligned} \tag{4.54}$$

4.4 Spherical Harmonics

As we will see in section 5, it is useful to express the wave in terms of spin-2 weighted spherical harmonics ${}_{-2}Y^{lm}(\theta,\varphi)$. The spherical harmonics are functions on S^2, and are eigenfunctions of the spherical part of the Laplacian. In spherical coordinates the Laplacian is given by

$$\nabla^2 f = \frac{1}{r^2}\frac{\partial}{\partial r}\left(r^2\frac{\partial f}{\partial r}\right) + \frac{1}{r^2\sin\theta}\frac{\partial}{\partial\theta}\left(\sin\theta\frac{\partial f}{\partial\theta}\right) + \frac{1}{r^2\sin^2\theta}\frac{\partial^2 f}{\partial\varphi^2}. \tag{4.55}$$

To define the spin-weighted spherical harmonics we will need the Wigner rotation matrix $d^l_{ms}(\theta)$. It is given by

$$\begin{aligned} d^l_{ms}(\theta) = &\sqrt{(l+m)!(l-m)!(l+s)!(l-s)!} \\ &\times \sum_{k=k_i}^{k_f}\frac{(-1)^k(\sin\frac{\theta}{2})^{2k+s-m}(\cos\frac{\theta}{2})^{2l+m-s-2k}}{k!(l+m-k)!(l-s-k)!(s-m+k)!}. \end{aligned} \tag{4.56}$$

Where $k_i = \max(0, m-s)$ and $k_f = \min(l+m, l-s)$. The spin-weighted spherical harmonics are then defined by

$${}_{-s}Y^{lm}(\theta,\varphi) = (-1)^s\sqrt{\frac{2l+1}{4\pi}}d^l_{ms}(\theta)e^{im\varphi}. \tag{4.57}$$

Next we define the waveform $h = h_+ - ih_\times$. We can then use the spin-weighted spherical harmonics of weight 2 to write h in the form of

$$h(t,\theta,\varphi) = \sum_{l=2}^{\infty}\sum_{m=-l}^{l} h^{lm}(t)\,{}_{-2}Y^{lm}(\theta,\varphi). \tag{4.58}$$

We will show this relation in section 5. We will use earlier work by E. Kidder [Law18] (p. 9) to find the prefactors h^{lm}. By using these spin-2 weighted spherial harmonics and writing our wave form up to 1.5 Post Newtonian order, we see that our prefactors become

$$h^{22} = -8\sqrt{\frac{\pi}{5}}\frac{G\mu}{rc^2}e^{-2i\omega t}x, \tag{4.59}$$

$$h^{21} = -\frac{8i}{3}\sqrt{\frac{\pi}{5}}\frac{G\mu\delta}{rc^2}e^{-i\omega t}x^{\frac{3}{2}}, \tag{4.60}$$

$$h^{33} = 3i\sqrt{\frac{6\pi}{7}}\frac{G\mu\delta}{rc^2}e^{-3i\omega t}x^{\frac{3}{2}}, \tag{4.61}$$

$$h^{31} = -\frac{i}{3}\sqrt{\frac{2\pi}{35}}\frac{G\mu\delta}{rc^2}e^{-i\omega t}x^{\frac{3}{2}}. \tag{4.62}$$

Here $x = (\frac{GM\omega}{c^3})^{\frac{2}{3}}$, and $\delta = \frac{m_1-m_2}{M}$. The prefactors for negative m are given using the relation $h^{l-m} = (-1)^l h^{lm*}$. All other factors and higher terms of these prefactors vanish because they are dependent on a higher order of x.

4.5 Stationary Phase Approximation

In the previous section we assumed that ω would be constant. However, in reality this is not the case. Let us write the phase as a function of time by $\Phi(t)$, Then as we saw in section 2 we can write the detectors incomming signal as

$$h(t) = F_+(\varphi,\theta,\psi)h_+(t) + F_\times(\varphi,\theta,\psi)h_\times(t), \tag{4.63}$$

where, if we only consider the dominant term we have that

$$h_+(t) = A(t)(1+\cos^2(\iota))\cos(\Phi(t)), \tag{4.64}$$

$$h_\times(t) = A(t)2\cos(\iota)\sin(\Phi(t)). \tag{4.65}$$

Then, using the fact that $\sin(\arctan(x)) = \frac{x}{\sqrt{1+x^2}}$ and $\cos(\arctan(x)) = \frac{1}{\sqrt{1+x^2}}$, we can rewrite h_+

$$h(t) = A(t)\sqrt{F_+^2(\cos^2(\iota)+1)^2 + F_\times^2 4\cos^2(\iota)}\cos(\Phi(t)+\varphi_0), \tag{4.66}$$

where $\varphi_0 = \arctan(\frac{-F_\times\cos(\iota)}{F_+(\cos^2(\iota)+1)})$. Like explained in section 3, in order to calculate the match we need to use the fourier transform of the waveform so that we can work in the frequency domain. If we apply this to eq. (4.66) we get

$$\int dt\, A(t)\cos(\Phi(t)+\varphi_0)e^{2\pi ft} = \frac{1}{2}\int dt\, A(t)(e^{i(\Phi(t)+\varphi_0)} + e^{-i(\Phi(t)+\varphi_0)})e^{2\pi ft}. \tag{4.67}$$

Now we make an approximation. $\Phi(t)$ must be monotonically increasing, because the binary black holes only rotate in one direction. On the other hand, in the other exponential

ft is also monotonically increasing. Which means that the first term, which goes by $e^{i(\Phi(t)+\varphi_0+2\pi ft)}$, will be a vector in $\mathbb{C}$ pointing in a random direction. When integrating over time, these vectors will cancel each other out, and we can approximate the integral over the first term by 0. In the other term however, the exponential goes with $2\pi ft-\Phi(t)$, which is not a monotonic increasing function. In fact, it will have a stationary point, which will contribute most to the integral. This is when $2\pi f = \dot{\Phi}(t)$. If we now taylor expand the exponant we get

$$\begin{aligned} 2\pi ft - \Phi(t) &= 2\pi ft_s - \Phi(t_s) + (2\pi f - \dot{\Phi}(t_s))(t-t_s) - \frac{1}{2}\ddot{\Phi}(t_s)(t-t_s)^2 + \dots \\ &= 2\pi ft_s - \Phi(t_s) - \frac{1}{2}\ddot{\Phi}(t_s)(t-t_s)^2. \end{aligned} \tag{4.68}$$

Let us use the change of variables $x = \sqrt{\frac{\ddot{\Phi}(t_s)}{2}}(t-t_s)$. Then the integral in eq. (4.67) becomes

$$\frac{1}{2}A(t_s(f))e^{-i\varphi_0}e^{i(2\pi ft_s(f)-\Phi(t_s(f)))}\sqrt{\frac{2}{\ddot{\Phi}(t_s(f))}}\int_{-\infty}^{\infty} dx\, e^{-ix^2}, \tag{4.69}$$

where $\int_{-\infty}^{\infty} dx\, d^{-ix^2} = \sqrt{\pi}e^{-i\frac{\pi}{4}}$. This gives us the result

$$\int dt\, A(t)\cos(\Phi(t)+\varphi_0)e^{2\pi ft} \approx \frac{\sqrt{\pi}}{2}A(t(f))\sqrt{\frac{2}{\ddot{\Phi}(t_s(f))}}e^{-i\varphi_0}e^{i\Psi(f)}, \tag{4.70}$$

where $\Psi(f) = 2\pi ft(f)-\Phi(t(f))-\frac{\pi}{4}$. When we also consider higher orders of the waveform, the stationary phase approximation gets extra terms as well. It turns out that even to approximate the waveform up to 0.5-PN order, we need the 3.5-PN order stationary phase approximation. We use the derivation from the paper ref. [KAs18] (eq. (3.3), p. 6). In the article they derive that the stationary phase approximation is given by

$$\Psi_{\text{SPA}}(f) = 2\pi ft_c - \varphi_c - \frac{\pi}{4} + \frac{3}{128\eta x^5}\sum_{k=0}^{7}\alpha_k x^k. \tag{4.71}$$

Here t_c is the time at coallesence and φ_c the rotation angle at coallesence. Furthermore, $x = (\frac{\pi GMf}{c^3})^{1/3}$, $\eta = \frac{m_1 m_2}{M^2}$, and the coefficients α_k, for $k = 0, \ldots, 7$ are given by

$$\alpha_0 = 1, \tag{4.72}$$

$$\alpha_1 = 0, \tag{4.73}$$

$$\alpha_2 = \frac{20}{9}\left(\frac{743}{336} + \frac{11}{4}\eta\right), \tag{4.74}$$

$$\alpha_3 = -16\pi, \tag{4.75}$$

$$\alpha_4 = 10\left(\frac{3058673}{1016064} + \frac{5429}{1008}\eta + \frac{617}{144}\eta^2\right), \tag{4.76}$$

$$\alpha_5 = \pi\left(\frac{38645}{756} + \frac{38645}{252}\log(\frac{x}{x_{\text{lso}}}) - \frac{65}{9}\eta\left[1 + 3\log(\frac{x}{x_{\text{lso}}})\right]\right), \tag{4.77}$$

$$\begin{aligned}\alpha_6 = &\left(\frac{11583231236531}{4694215680} - \frac{640\pi^2}{3} - \frac{6848\gamma}{21}\right) \\ &+ \eta\left(-\frac{15335597827}{3048192} + \frac{2255\pi^2}{12} - \frac{1760\theta}{3} + \frac{12320\lambda}{9}\right) \\ &+ \frac{76055}{1728}\eta^2 - \frac{127825}{1296}\eta^3 - \frac{6848}{21}\log(4x),\end{aligned} \tag{4.78}$$

$$\alpha_7 = \pi\left(\frac{77096675}{254016} + \frac{378515}{1512}\eta - \frac{74045}{756}\eta^2\right). \tag{4.79}$$

Here x_{lso} is the value of x in the last stable orbit. The frequency of the last stable orbit is given by $f_{\text{lso}} = \frac{c^3}{(6^{2/3}\pi GM)}$, so $x_{\text{lso}} = 6^{-2/9}$. The values of the parameters θ and λ have recently been determined to the values $\lambda = -\frac{1987}{3080}$ and $\theta = -\frac{11831}{9240}$ according to [KAs18] (p. 7). Finally, γ is the Euler's constant and is given by $\gamma = 0.577\ldots$.

Now we can find the fourier transform of eq. (4.58). This becomes

$$\tilde{h}(f, \theta, \varphi) = \sum_{l=2}^{\infty}\sum_{m=-l}^{l} \tilde{h}^{lm}(f)\, {}_{-2}Y^{lm}(\theta, \varphi). \tag{4.80}$$

We will also need the fourier transforms of the prefactors of the exponent in equations (4.59) -(4.62). We will use the paper [Mis16] (p. 5-6) to find these. According to this article the $\tilde{h}_{lm}$ terms are given by

$$\tilde{h}_{lm} = \frac{G^2M^2}{D_L c^7}\pi\sqrt{\frac{2\eta}{3}}V_m^{-7/2}e^{-i(m\Psi_{\text{SPA}}(f)+\pi/4)}H_{lm}(V_m). \tag{4.81}$$

Here $V_m = (\frac{2\pi GMf}{mc^3})^{1/3}$, and D_L stands for the luminosity distance. The factors H_{lm} up to 0.5 PN order, are given by

$$H_{22}(V_2) = -1, \tag{4.82}$$

$$H_{21}(V_1) = -\frac{\sqrt{2}}{3}\delta V_1, \tag{4.83}$$

$$H_{33}(V_3) = -\frac{3}{4}\sqrt{\frac{5}{7}}\delta V_3, \tag{4.84}$$

$$H_{31}(V_1) = -\frac{1}{12\sqrt{7}}\delta V_1. \tag{4.85}$$

Again, we find the coefficient for negative m using $\tilde{h}_{l-m} = (-1)^l \tilde{h}^*_{lm}$.

5 Spin-weighted Spherical Harmonics

As we saw in section 4, we can express the waveform in terms of spin-2 weighted spherical harmonics. However, now the question arises why this can be done. We may do this because we can express the waveform in terms of tensor spherical harmonics, which in their turn are related to spin-2 spherical harmonics. In this section we will show how the spin-weighted spherical harmonics are defined and how they are related to gravitational waves caused by binary black holes. In the end we will find the following equation

$$h_+ - h_\times = \sum_{l=2}^{\infty} \sum_{m=-l}^{l} h_{lm} \, {}_{-2}Y^{lm}. \tag{5.1}$$

5.1 The regular spherical harmonics

To define the spin-weighted spherical harmonics we of course need the spherical harmonics. The spherical harmonics are defined using the associated Legendre polynomials $P^{lm}(x)$. As written in [LB07] on page 320, the associated Legendre functions $P_l^m(x)$ are given by

$$P_l^m(x) = \frac{1}{2^l l!}(1-x^2)^{m/2}\frac{d^{m+l}}{dx^{m+l}}(x^2-1)^l. \tag{5.2}$$

Additionally, in [LB07] it is specified how the spherical harmonics are related to the associated legendre polynomials by

$$Y_l^m(\theta,\varphi) = (-1)^m \sqrt{\frac{2l+1}{4\pi}\frac{(l-m)!}{(l+m)!}} P_l^m(\cos\theta) e^{im\varphi}. \tag{5.3}$$

Note that the spherical harmonics are eigenfunctions of the Laplacian. We can also derive them this way. If we consider a consider a scalar field f of which the Laplacian is zero. So

$$\nabla^2 f = \frac{1}{r^2}\frac{\partial}{\partial r}\left(r^2\frac{\partial f}{\partial r}\right) + \frac{1}{r^2\sin\theta}\frac{\partial}{\partial\theta}\left(\sin\theta\frac{\partial f}{\partial\theta}\right) + \frac{1}{r^2\sin^2\theta}\frac{\partial^2 f}{\partial\varphi^2} = 0. \tag{5.4}$$

We then assume that this scalar field exists out of a radial part $R(r)$ and an angular part $Y(\theta,\varphi)$. Therefore, $f(r,\theta,\varphi) = R(r)\,Y(\theta,\varphi)$. Now we can split 5.4 into two separate differential equations. By multiplying by r^2 and dividing by f we find

$$\frac{1}{R}\frac{\partial}{\partial r}\left(r^2\frac{\partial R}{\partial r}\right) = \lambda, \tag{5.5}$$

$$\frac{1}{Y\sin\theta}\frac{\partial}{\partial\theta}\left(\sin\theta\frac{\partial Y}{\partial\theta}\right) + \frac{1}{Y\sin^2\theta}\frac{\partial^2 Y}{\partial\varphi^2} = -\lambda. \tag{5.6}$$

Where λ is a complex constant. Eq. (5.6) can be simplified by again assuming that $Y(\theta,\varphi) = \Theta(\theta)\Phi(\varphi)$. By applying separation of variables and multiplying by $\sin^2\theta$ and

dividing by Y we find

$$\frac{1}{\Phi}\frac{d^2\Phi}{d\varphi^2} = -m^2, \tag{5.7}$$

$$\lambda \sin^2\theta + \frac{\sin\theta}{\Theta}\frac{d}{d\theta}\left(\sin\theta\frac{d\Theta}{d\theta}\right) = m^2. \tag{5.8}$$

Where again, m is a complex constant. We know that Φ is a periodic function and that it's period devides 2π. Therefore, m must be an integer. Furthermore we know that Φ is a linear combination of the functions $e^{\pm im\varphi}$. If we now assume that λ can be written in the form $l(l+1)$. Then, using eq. (5.6) we find that

$$\frac{1}{\Theta\sin\theta}\frac{d}{d\theta}\left(\sin\theta\frac{d\Theta}{d\theta}\right) - \frac{m^2}{\sin^2\theta} = -l(l+1). \tag{5.9}$$

If we use a coordinate transformation $y = \Theta(\theta)$ and $x = \cos\theta$ we can rewrite this to

$$\frac{1}{y}\frac{d}{dx}\left((1-x^2)\frac{dy}{dx}\right) - \frac{m^2}{\sin^2\theta} = -l(l+1). \tag{5.10}$$

Therefore, we get

$$-2x\frac{dy}{dx} + (1-x^2)\frac{d^2y}{dx^2} + \left[l(l+1) - \frac{m^2}{1-x^2}\right]y = 0. \tag{5.11}$$

This is exactly how the associated Legandre polynomials are defined. So, $y(x) = P_l^m(x)$ for $l = 0, 1, 2, 3, \ldots$ and $m = -l, -l+1, \ldots, l$. Therefore, we see that $\Theta(\theta) = P_l^m(\cos(\theta))$ and $\Phi(\varphi) = e^{im\varphi}$. We conclude that

$$Y^{lm}(\theta,\varphi) = C_{lm}P_l^m(\cos(\theta))e^{im\varphi}. \tag{5.12}$$

Where C_{lm} is a normalization constant.

5.2 Tensor spherical harmonics

The spherical harmonics which we derived above are extremely useful to describe the angular dependencies of a scalar field. Likewise, we can define tensor spherical harmonics, which are useful when describing the angular dependencies of a tensor field. We will need these tensor spherical harmonics to prove our main result 1.1 in the next subsection. There we link the spin-weighted spherical harmonics to our multipole expansion of the gravitational wave.

To define the tensor spherical harmonics we will need to make use of a few opperators. These include the orbital angular momentum operator $\mathbf{L}$, the spin operator $\mathbf{S}$ and the total angular momentum operator $\mathbf{J} = \mathbf{L} + \mathbf{S}$. According to [Mag08] on p. 144, the

opperators $\mathbf{J}^2, J_z, \mathbf{L}^2, \mathbf{S}^2$ all commute and are self-adjoint. Therefore, we can diagonalize them simultaneously. The eigenfunctions are the tensor spherical harmonics which we denote by $Y^{ls}_{jj_z}$. By definition, these functions are solutions of

$$\mathbf{J}^2 Y^{ls}_{jj_z} = j(j+1)Y^{ls}_{jj_z} \tag{5.13}$$
$$J_z Y^{ls}_{jj_z} = j_z Y^{ls}_{jj_z} \tag{5.14}$$
$$\mathbf{L}^2 Y^{ls}_{jj_z} = l(l+1)Y^{ls}_{jj_z} \tag{5.15}$$
$$\mathbf{S}^2 Y^{ls}_{jj_z} = s(s+1)Y^{ls}_{jj_z}. \tag{5.16}$$

We can express them explicitly by coupling the scalar spherical harmonics Y_{lm} to the spin function χ_{ss_z}. This has to be done with the aid of the proper Clebsch-Gordan coefficient. The Clebsch-Gordan Coefficient couples a state with orbital angular momentum $|ll_z\rangle$ to a state with spin $|ss_z\rangle$ to get a state with total angular momentum $|jj_z\rangle$. They have a complicated expression given by

$$\begin{aligned}
&\langle j_1 m_1 j_2 m_2 | JM\rangle = \\
&\delta_{M,m_1+m_2}\sqrt{\frac{(2J+1)(J+j_1-j_2)!(J-j_1+j_2)!(j_1+j_2-J)!}{(j_1+j_2+J+1)!}}\times \\
&\sqrt{(J+M)!(J-M)!(j_1-m_1)!(j_1+m_1)!(j_2-m_2)!(j_2+m_2)!}\times \\
&\sum_k \frac{(-1)^k}{k!(j_1+j_2-J-k)!(j_1-m_1-k)!(j_2+m_2-k)!(J-j_2+m_1+k)!(J-j_1-m_2+k)!}
\end{aligned} \tag{5.17}$$

We use this to define the tensor spherical harmonics

$$Y^{ls}_{jj_z} = \sum_{l_z=-l}^{l}\sum_{s_z=-s}^{s} \langle s l s_z l_z | j j_z\rangle Y_{ll_z}\chi_{ss_z}. \tag{5.18}$$

$\mathbf{L}^2$ only works on the variables θ and φ. Therefore, $\mathbf{L}^2$ only works on Y_{ll_z}. Y_{ll_z} has the porperty that $\mathbf{L}^2 Y_{ll_z} = l(l+1)Y_{ll_z}$ and eq. (5.15) follows. Likewise, $\mathbf{S}^2$ only works on χ_{ss_z}, for which holds that $\mathbf{S}^2\chi_{ss_z} = s(s+1)\chi_{ss_z}$ and we find eq. (5.16). Finally, $\mathbf{J}^2$ and J_z only work on $|jj_z\rangle$. These operators have the porperty that $\mathbf{J}^2|jj_z\rangle = j(j+1)|jj_z\rangle$ and $J_z|jj_z\rangle = j_z|jj_z\rangle$. The equations (5.13) and (5.14) follow.

For gravitational waves, the tensor spherical harmonics of spin 2 are of importance. In order to define the tensor spherical harmonics of spin 2, we first need to define an appropriate spin function. We will let the spin-2 function be a linear combination of tensor products of spin-1 fucntions. As spin-1 functions we define

$$\xi^{(\pm 1)} = \mp\frac{1}{\sqrt{2}}(\mathbf{e}_x \pm i\mathbf{e}_y),\ \ \xi^{(0)} = \mathbf{e}_z. \tag{5.19}$$

We will denote the spin-2 function by $t_{ik}^{(s_z)}$ and the function will match a vector $\xi^{(m_1)}$ with $\xi^{(m_2)}$ and with the appropriate Clebsch-Gordan coëfficient. We get

$$t_{ik}^{(s_z)} = \sum_{m_1,m_2=-1}^{1} \langle 11 m_1 m_2 | 2 s_z \rangle \xi_i^{(m_1)} \xi_k^{(m_2)}. \tag{5.20}$$

All five tensors, for $s_z = \pm 2, \pm 1, 0$, are symmetric and traceless. To see this, it is clear that $t_{ik}^{(s_z)}$ is symmetric from the definition . It is traceless as well, since for the Clebsch-Gordan coëfficient to be non-zero we have that $m_1 + m_2 = s_z$. Therefore, using eq. (5.20)

$$t_{ii}^{(\pm 2)} = \langle 11(\pm 1)(\pm 1) | 2(\pm 2) \rangle \xi_i^{(\pm 1)} \xi_i^{(\pm 1)} = 0, \qquad \text{(Because } \xi_i^{(\pm 1)} \xi_i^{(\pm 1)} = 0) \tag{5.21}$$

$$\tag{5.22}$$

$$\begin{aligned} t_{ii}^{(\pm 1)} &= \langle 11(\pm 1)0 | 2(\pm 1) \rangle \xi_i^{(\pm 1)} \xi_i^{(0)} \\ &+ \langle 110(\pm 1) | 2(\pm 1) \rangle \xi_i^{(0)} \xi_i^{(\pm 1)} = 0, \qquad \text{(Because } \xi_i^{(\pm 1)} \xi_i^{(0)} = 0) \end{aligned} \tag{5.23}$$

$$\tag{5.24}$$

$$\begin{aligned} t_{ii}^{(0)} &= \langle 111(-1) | 20 \rangle \xi_i^{(1)} \xi_i^{(-1)} \\ &+ \langle 1100 | 20 \rangle \xi_i^{(0)} \xi_i^{(0)} \\ &+ \langle 11(-1)1 | 20 \rangle \xi_i^{(-1)} \xi_i^{(1)} \\ &= -\sqrt{\frac{1}{6}} + \sqrt{\frac{2}{3}} - \sqrt{\frac{1}{6}} = 0.. \end{aligned} \tag{5.25}$$

Using this symmetric and traceless spin tensor we define the spin-2 tensor harmonics by

$$(\mathbf{T}^l_{jj_z})_{ik} = (\mathbf{Y}^{l2}_{jj_z})_{ik} = \sum_{l_z=-l}^{l} \sum_{s_z=-2}^{2} \langle 2 l s_z l_z | j j_z \rangle Y_{l l_z} t_{ik}^{(s_z)}. \tag{5.26}$$

The spin-2 harmonics is non-zero if $|2 - l| \leq j \leq 2 + l$. Furthermore, they are eigen-funcitions of $\mathbf{L}^2$, but have no relation to the radial vector $\hat{\mathbf{n}}$. Using the full set of tensors however, we can define linear combinations of the tensor harmonics which are related to

the radial vector and rotations around this vector. For $j \geq 2$ we define

$$\mathbf{T}^{S0}_{jj_z} = \left(\frac{(j+1)(j+2)}{(2j+1)(2j+3)}\right)^{1/2} \mathbf{T}^{j+2}_{jj_z} - \left(\frac{2j(j+1)}{3(2j-1)(2j+3)}\right)^{1/2} \mathbf{T}^{j}_{jj_z} + \left(\frac{(j-1)j}{(2j-1)(2j+1)}\right)^{1/2} \mathbf{T}^{j-2}_{jj_z}, \tag{5.27}$$

$$\mathbf{T}^{E1}_{jj_z} = -\left(\frac{2j(j+2)}{(2j+1)(2j+3)}\right)^{1/2} \mathbf{T}^{j+2}_{jj_z} - \left(\frac{3}{3(2j-1)(2j+3)}\right)^{1/2} \mathbf{T}^{j}_{jj_z} + \left(\frac{2(j-1)(j+1)}{(2j-1)(2j+1)}\right)^{1/2} \mathbf{T}^{j-2}_{jj_z}, \tag{5.28}$$

$$\mathbf{T}^{E2}_{jj_z} = \left(\frac{(j-1)j}{2(2j+1)(2j+3)}\right)^{1/2} \mathbf{T}^{j+2}_{jj_z} + \left(\frac{3(j-1)(j+1)}{(2j-1)(2j+3)}\right)^{1/2} \mathbf{T}^{j}_{jj_z} + \left(\frac{(j+1)(j+3)}{2(2j-1)(2j+1)}\right)^{1/2} \mathbf{T}^{j-2}_{jj_z}, \tag{5.29}$$

$$\mathbf{T}^{B1}_{jj_z} = \left(\frac{j+2}{2j+1}\right)^{1/2} \mathbf{T}^{j+1}_{jj_z} - \left(\frac{j-1}{2j+1}\right)^{1/2} \mathbf{T}^{j-1}_{jj_z}, \tag{5.30}$$

$$\mathbf{T}^{B2}_{jj_z} = -\left(\frac{j-1}{(2j+1)}\right)^{1/2} \mathbf{T}^{j+1}_{jj_z} - \left(\frac{j+21}{2j+1}\right)^{1/2} \mathbf{T}^{j-1}_{jj_z}. \tag{5.31}$$

Both Maggiore [Mag08] (p. 149) and Thorne [Tho80] (p. 311) give relations between these tensor harmonics and the spherical harmonics. Unfortunately, we were not able to proof these relations. However we will use them later on. These are given by

$$(\mathbf{T}^{S0}_{jj_z})_{ik} = [n_i n_k - \frac{1}{3}\delta_{ik}]Y_{jj_z}, \tag{5.32}$$

$$(\mathbf{T}^{E1}_{jj_z})_{ik} = c^{(1)}_j \frac{r}{2}(n_i\partial_k + n_k\partial_i)Y_{jj_z}, \tag{5.33}$$

$$(\mathbf{T}^{E2}_{jj_z})_{ik} = c^{(2)}_j r^2 \Lambda_{ik,i'k'}(\hat{\mathbf{n}})\partial_{i'}\partial_{k'}Y_{jj_z}, \tag{5.34}$$

$$(\mathbf{T}^{B1}_{jj_z})_{ik} = c^{(1)}_j (\frac{i}{2})(n_i L_k + n_k L_i)Y_{jj_z}, \tag{5.35}$$

$$(\mathbf{T}^{B2}_{jj_z})_{ik} = c^{(2)}_j r\Lambda_{ik,i'k'}(\hat{\mathbf{n}})(\frac{i}{2})(\partial_{i'}L_{k'} + \partial_{k'}L_{i'})Y_{jj_z}. \tag{5.36}$$

Where $c^{(1)}_j = (\frac{2}{j(j+1)})^{\frac{1}{2}}$ and $c^{(2)}_j = (2\frac{(l-2)!}{(l+2)!})^{\frac{1}{2}}$. By construction all tensor spherical harmonics are symmetric as well as traceless. Nevertheless, note that only $\mathbf{T}^{E2}_{jj_z}$ and $\mathbf{T}^{B2}_{jj_z}$ are transverse. Or in other words $n_i(\mathbf{T}^{E2}_{jj_z})_{ik} = 0$ and $n_i(\mathbf{T}^{B2}_{jj_z})_{ik} = 0$, because $n_i\Lambda_{ik,i'k'}(\hat{\mathbf{n}}) = 0$. Since our gravitational wave expression is transverse, we can conclude that only the $\mathbf{T}^{E2}_{jj_z}$ and the $\mathbf{T}^{B2}_{jj_z}$ terms enter the expression for our wave h^{TT}_{ij}. As discussed in [Mag08], the wave becomes of the form

$$h^{TT}_{ij} = \sum_{l=2}^{\infty}\sum_{m=-l}^{l} u_{lm}(\mathbf{T}^{E2}_{lm})_{ij}(\theta,\varphi) + v_{lm}(\mathbf{T}^{B2}_{lm})_{ij}(\theta,\varphi). \tag{5.37}$$

Here u_{lm} and v_{lm} are functions of retarded time $t - \frac{r}{c}$ and of the distance to the observer r.

5.3 Spin weighted spherical harmonics

Now we know that we can express the transverse traceless wave in terms of tensor spherical harmonics, we will find a relation between tensor harmonics and spin-2 spherical harmonics. First let us define the waveform as

$$h := h_+ - ih_\times. \tag{5.38}$$

h_+ and $h_\times$ are both real valued. Therefore, we can do calculations with h and still retract the values of h_+ and $h_\times$, since $h_+ = \mathrm{Re}(h)$ and $h_\times = \mathrm{Im}(h)$. Furthermore we will use that the spherical harmonics from eq. (5.3) have spin weight 0. Then we define the spin lowering operator $\bar{\eth}$ which works on a function of spin weight s as

$$\bar{\eth} := -(\sin\theta)^{-s}\left[\frac{\partial}{\partial\theta} - i\frac{1}{\sin\theta}\frac{\partial}{\partial\varphi}\right](\sin\theta)^s. \tag{5.39}$$

This operator lowers the spin weight by one. Since the spherical harmonics have spin weight 0, we can define the spin-2 weighted spherical harmonics by

$${}_{-2}Y^{lm}(\theta,\varphi) = (\frac{(l-2)!}{(l+2)!})^{\frac{1}{2}}\bar{\eth}^2\, Y^{lm}(\theta,\varphi). \tag{5.40}$$

In this section we will prove that there exists coefficients h^{lm} that depend on the retarded time $t - \frac{r}{c}$ and the distance to the observer r, such that the waveform can be expressed in terms of spin-2 weighted spherical harmonics by

$$h_+ - ih_\times = \sum_{l=2}^{\infty}\sum_{m=-l}^{l} h^{lm}\,{}_{-2}Y^{lm}. \tag{5.41}$$

The spin weighted spherical harmonics are described by Goldberg in [GMN+67]. Here Goldberg uses a spin raising operator $\eth$ and spin lowering operator $\bar{\eth}$ to induce spin weight on functions. What it means for a function to be of spin weight s is not important for our purpose. Nevertheless, we can use these operators to define the spin weighted spherical harmonics which we will need. The spin raising operator when working on a function η of spin weight s is defined using the following formula

$$\eth\eta = -(\sin\theta)^{s}\left[\frac{\partial}{\partial\theta} + i\frac{1}{\sin\theta}\frac{\partial}{\partial\varphi}\right](\sin\theta)^{-s}\eta. \tag{5.42}$$

Similarly, we can define it's complex conjugate the spin lowering operator as

$$\bar{\eth}\eta = -(\sin\theta)^{-s}\left[\frac{\partial}{\partial\theta} - i\frac{1}{\sin\theta}\frac{\partial}{\partial\varphi}\right](\sin\theta)^{s}\eta. \tag{5.43}$$

It turns out that $\eth$ raises the spin by 1. Therefore, if η has spin-weight s, then $\eth\eta$ has spin weight $s+1$. Likewise, $\bar{\eth}\eta$ has spin $s-1$.

Now we can look at the effect of $\eth$ on the spherical harmonics. We can define spin-s weighted spherical harmonics as

$$ {}_sY^{lm} = \begin{cases} \left(\frac{(l-s)!}{(l+s)!}\right)^{\frac{1}{2}} \eth^s Y^{lm} & \text{if } 0 \leq s \leq l \\ \left(\frac{(l+s)!}{(l-s)!}\right)^{\frac{1}{2}} (-1)^s \bar{\eth}^{-s} Y^{lm} & \text{if } -l \leq s \leq 0 \end{cases}. \tag{5.44} $$

Now we can try to find a relation between the tensor spherical harmonics from section 5.2 and the spin weighted spherical harmonics. Let us first define a complex vector $\mathbf{m}$ that will help us find this relation. We define

$$ \mathbf{m} := \frac{1}{\sqrt{2}}(\mathbf{e}_\theta + i\mathbf{e}_\varphi) \tag{5.45} $$

According to [Law18] and [Tho80], the tensor harmonics are related to the spin-2 spherical harmonics by

$$ \mathbf{T}^{E2,lm}_{ij} = \frac{1}{\sqrt{2}}(m_i m_j \, {}_{-2}Y^{lm} + m_i^* m_j^* \, {}_2Y^{lm}) \tag{5.46} $$

$$ \mathbf{T}^{B2,lm}_{ij} = \frac{-i}{\sqrt{2}}(m_i m_j \, {}_{-2}Y^{lm} - m_i^* m_j^* \, {}_2Y^{lm}). \tag{5.47} $$

Here $m_i m_j$ represents the tensor product of $\mathbf{m}$ with itself, $\mathbf{m} \otimes \mathbf{m}$. We will now prove this relation. First of all we will express the spin-2 weighted spherical harmonics in terms of regular spherical harmonics. Using definition 5.44 and 5.42 we can write out the spin-2 weighted spherical harmonic as

$$ \begin{aligned} {}_2Y^{lm} &= \left(\frac{(l-2)!}{(l+2)!}\right)^{\frac{1}{2}} \eth^2 Y^{lm} \\ &= \left(\frac{(l-2)!}{(l+2)!}\right)^{\frac{1}{2}} \eth \left[-\frac{\partial}{\partial\theta} - i\frac{1}{\sin\theta}\frac{\partial}{\partial\varphi}\right] Y^{lm} \\ &= \left(\frac{(l-2)!}{(l+2)!}\right)^{\frac{1}{2}} (-\sin\theta) \left[\frac{\partial}{\partial\theta} + i\frac{1}{\sin\theta}\frac{\partial}{\partial\varphi}\right] \frac{1}{\sin\theta} \left[-\frac{\partial}{\partial\theta} - i\frac{1}{\sin\theta}\frac{\partial}{\partial\varphi}\right] Y^{lm}. \end{aligned} \tag{5.48} $$

After some simplifications we will find that this becomes

$$ {}_2Y^{lm} = \left(\frac{(l-2)!}{(l+2)!}\right)^{\frac{1}{2}} \left[-\frac{\cos\theta}{\sin\theta}\frac{\partial}{\partial\theta} - 2i\frac{\cos\theta}{\sin^2\theta}\frac{\partial}{\partial\varphi} + \frac{\partial^2}{\partial\theta^2} + 2i\frac{1}{\sin\theta}\frac{\partial^2}{\partial\theta\partial\varphi} - \frac{1}{\sin^2\theta}\frac{\partial^2}{\partial\varphi^2}\right] Y^{lm}. \tag{5.49} $$

Likewise we can write the spin-(-2) weighted spherical harmonics as

$$\begin{aligned}
{}_{-2}Y^{lm} &= \left(\frac{(l-2)!}{(l+2)!}\right)^{\frac{1}{2}} \bar{\eth}^2 Y^{lm} \\
&= \left(\frac{(l-2)!}{(l+2)!}\right)^{\frac{1}{2}} \bar{\eth}\left[-\frac{\partial}{\partial\theta} + i\frac{1}{\sin\theta}\frac{\partial}{\partial\varphi}\right] Y^{lm} \\
&= \left(\frac{(l-2)!}{(l+2)!}\right)^{\frac{1}{2}} (-\sin\theta)\left[\frac{\partial}{\partial\theta} - i\frac{1}{\sin\theta}\frac{\partial}{\partial\varphi}\right]\frac{1}{\sin\theta}\left[-\frac{\partial}{\partial\theta} + i\frac{1}{\sin\theta}\frac{\partial}{\partial\varphi}\right] Y^{lm} \\
&= \left(\frac{(l-2)!}{(l+2)!}\right)^{\frac{1}{2}} \left[-\frac{\cos\theta}{\sin\theta}\frac{\partial}{\partial\theta} + 2i\frac{\cos\theta}{\sin^2\theta}\frac{\partial}{\partial\varphi} + \frac{\partial^2}{\partial\theta^2} - 2i\frac{1}{\sin\theta}\frac{\partial^2}{\partial\theta\partial\varphi} - \frac{1}{\sin^2\theta}\frac{\partial^2}{\partial\varphi^2}\right] Y^{lm}.
\end{aligned} \tag{5.50}$$

We can substitute this into eq. (5.46) and (5.47). Now the right hand side of the eq. (5.46) in terms of spherical coordinates becomes

$$\frac{1}{[2l(l-1)(l+1)(l+2)]^{\frac{1}{2}}}\begin{pmatrix} 0 & 0 & 0 \\ 0 & A^{lm} & B^{lm} \\ 0 & B^{lm} & -A^{lm} \end{pmatrix}. \tag{5.51}$$

Where A^{lm} and B^{lm} are given by

$$A^{lm} = \left[-\frac{\cos\theta}{\sin\theta}\frac{\partial}{\partial\theta} + \frac{\partial^2}{\partial\theta^2} - \frac{1}{\sin^2\theta}\frac{\partial^2}{\partial\varphi^2}\right] Y^{lm} \tag{5.52}$$

$$B^{lm} = 2\frac{\partial}{\partial\varphi}\left[\frac{1}{\sin\theta}\frac{\partial}{\partial\theta} - \frac{\cos\theta}{\sin^2\theta}\right] Y^{lm}. \tag{5.53}$$

This equation coincides with the one that Thorne [Tho80] and Zerilli [Zer70] (p. 2207) found for $\mathbf{T}^{E2,lm}$. Note that in the notation by [Zer70], $\mathbf{T}^{E2,lm} = \mathbf{f}_{lm}$ and $\mathbf{T}^{B2,lm} = i\mathbf{d}_{lm}$. Therefore we conclude that eq. (5.46) is true. Therefore we found a relation between $\mathbf{T}^{E2,lm}$ and the spin-2 weighted spherical harmonics. Equivilantly, on the right hand side of eq. (5.47) we find

$$\frac{1}{[2l(l-1)(l+1)(l+2)]^{\frac{1}{2}}}\begin{pmatrix} 0 & 0 & 0 \\ 0 & B^{lm} & A^{lm} \\ 0 & A^{lm} & -B^{lm} \end{pmatrix}. \tag{5.54}$$

According to [Tho80], $\mathbf{T}^{B2,lm}$ corresponds in Zerilli's article with $i\mathbf{d}_{lm}$. We note that also (5.54) corresponds with $i\mathbf{d}_{lm}$ from [Zer70]. Therefore, we conlcude that also eq. (5.47) is correct.

What rests us, is to rewrite the waveform in terms of spin-2 spherical harmonics. We can do this by using the relation [Law18]

$$h_+ - ih_\times = m_i^* m_j^* h_{ij}^{TT}. \tag{5.55}$$

Then we can combine equations 5.37, 5.46, 5.47 and 5.55 to finally find the main result

$$h_+ - ih_\times = \sum_{l=2}^{\infty} \sum_{m=-l}^{l} \left[\frac{1}{\sqrt{2}} u^{lm} - \frac{i}{\sqrt{2}} v^{lm} \right] {}_{-2}Y^{lm}. \tag{5.56}$$

Note that the positive spin weighted part completely dropped out because $m_i^* m_i^* = 0$. Therefore, we are only left with the negative spin weighted spherical harmonics. We conclude that there exist coefficients h^{lm} that depend on the retarted time t_r and the distance to the observer r such that eq. (5.41) holds. We can use this to simplify the expression of our waveform. This will not only make calculations easier but will also allow us to compare the waveform over the entire sphere, instead of just in the radial direction.

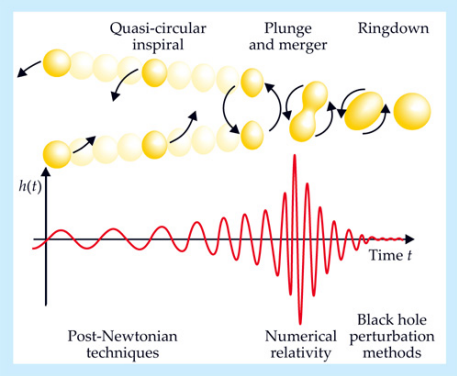

Figure 9: The three different phases during coalescence of binary black holes. Note that different techniques are needed to model different phases. [BS10]

6 State of the art waveform models

Now all the calculations are done, the waveform needs to be programmed in order to do data analysis. This was done using Python. There exists a useful library for python that has all the functions we need already ready programmed for us. This library is called PyCBC. Complicated calculations like the match in eq. (3.19), and waveforms are already programmed in this library and we will use them for our purpose.

6.1 Inspiral, merger, ringdown

There are several models already programmed in PyCBC. There exist different models for different phases, but we are mostly interested in the IMR waveforms. IMR stands for inspiral, merger, ringdown, which are the three phases during coalescence of binary black holes. In this subsection we show how we can model the three different phases and how they differ from each other. There are four ways to finding a correct describtion of the phases. There is the Post-Newtonian formalism, solving the Einstein equations by directly integrating, the effective one-body formalism, and the phenomenological waveforms

First of all, we will look at the Post-Newtonian techniques, which are used for inspiral. Here we expand general relativistic equations of motions in terms of v/c. This has as a consequence that the approximations are only valid up until $\frac{v}{c} \sim 0.1$. Nevertheless, it can be used to describe the start of the inspiral phase.

Next, we will look at the effective one body problem. Here we change the two body problem where the black holes rotate around the centre of mass, to a problem where one of the black holes stays still in the origin with a mass equal to the total mass M, and the other black hole rotates around the origin with a mass equal to the reduced mass μ

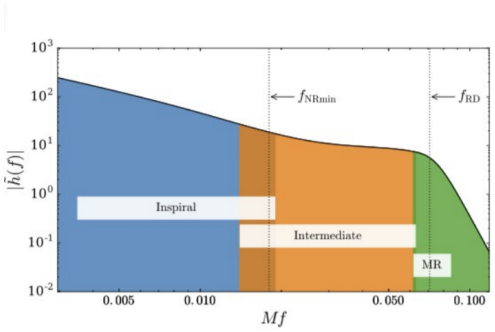

waveform regime	parameter	$f-$dependence
early-inspiral	φ_0	$f^{-5/3}$
	φ_1	$f^{-4/3}$
	φ_2	f^{-1}
	φ_3	$f^{-2/3}$
	φ_4	$f^{-1/3}$
	φ_{5l}	$\log f$
	φ_6	$f^{1/3}$
	φ_{6l}	$f^{1/3}\log f$
	φ_7	$f^{2/3}$
late-inspiral	σ_2	$f^{4/3}$
	σ_3	$f^{5/3}$
	σ_4	f^2
intermediate	β_2	$\log f$
	β_3	f^{-3}
merger-ringdown	α_2	f^{-1}
	α_3	$f^{3/4}$
	α_4	$\tan^{-1}(af+b)$

Figure 10: The phenom waveform exist out of different regimes. For each regime it has different parameters that have different frequency dependencies.

[BD99]. This leads to an effective metric

$$ds^2_{\rm eff} = -A(r)dt^2 + \frac{D(r)}{A(r)}dr^2 + r^2(d\theta^2 + \sin^2\theta d\varphi). \tag{6.1}$$

Eventhough, this is a technique copied from Newtonian problems and this does not give a solution to the Einstein equations, it does give a good approximation for the phase and motion of the coalescening binary black holes.

Thirdly, we can use numerical relativity. Here we split the Einstein equations in spatial and time parts, which is also called the $3+1$ formalism. Then these equations are solved numerically using computers [Pre05]. This technique give very precise estimations for inspiral, merger and ringdown. However, it takes weeks to just get one waveform.

Finally we have the phenomenological waveforms. As we can see in figure 10, in this describtion the coalescence process is split up in different regimes. Each regime is then described with the aid of different phase and amplitude functions that have various frequency dependencies. For the inspiral regime, also Post-Newtonian techniques are used, and for other regimes also parts of numerical tactics are used. In the end the waveform is of a similar quality of that of the effective one body problem. However, it is quickly generated using computers.

6.2 IMRPhenomHM

The IMRPhenomHM from the PyCBC library is an example of a phenomenological waveform. It is an extension of the PhenomD waveform [Lea18], another Phenomenological waveform that only conatians the $l = 2$, $m = 2$ mode. Even if the mass ratio is $1/3$, including higher harmonics in data analysis is beneficial. Therefore, surely for our purpose we should use a waveform that also includes the higher harmonics.

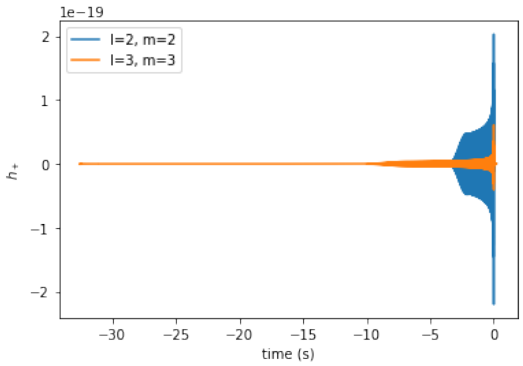

Figure 11: The IMRPhenomHM waveform from the PyCBC library in the time domain. In one of the waves only the $l = 2, m = 2$ is included, and in the other the $l = 3, m = 3$ mode is included. Furthermore, we set $\iota = \frac{\pi}{3}$, $m_1 = 30$, $m_2 = 10$.

The PhenomHM waveform gives analytical results close to waveforms that were calculated using numerical relativity [Lea18]. However, as mentioned in the previous section a phenomenological waveform is much quicker calculated than a waveform that is generated using numerical relativity. When we call the IMRPhenomHM waveform using python we can set the values for all parameters. We can even filter the modes. An example of this is given in figure 11.

There are several waveforms already available. However, there is also the possibility to define a waveform yourself. These waveforms can be either in the time domain or frequency domain. For our purpose we will work in the frequency domain. We can use the match function of PyCBC to test our own waveform against the IMRPhenomHM waveform. By making a selection of modes of the IMRPhenomHM function, we can test if our own modes are correct. For example, we can choose to just include the $l = 2, m = 2$ mode and $l = 3, m = 3$ mode into the waveform.

In order to compare two waveforms we have to use the match function. The match was defined in eq. (3.19). Here it was for neighbouring points. However we can also use it to compare a waveform $h(\bar{\theta})$ with another waveform $g(\bar{\theta})$ by

$$M = (\hat{h}(\bar{\theta})|\hat{g}(\bar{\theta})). \tag{6.2}$$

Here again $\hat{h} = \frac{h}{\sqrt{(h|h)}}$ and likewise for $\hat{g}$. If our waveform gives a match value close to 1 with the corresponding IMRPhenomHM waveform, then we programmed it correctly.

7 Testing general relativity with harmonics

Everything up untill now that we have based the equation of our waveform on comes from general relativity. However, how can we be so certain that this theory is correct? There are many conflicts between general relativity and quantum mechanics [Wig97]. Therefore, we have to keep on testing the theory for different inaccuracies. A way to do this is with parameterized tests. In this section we will look at what a parameterized test is and how they have been used in the past to test general relativity. After this we will look at how we can use it to test general relativity in a new way and what deviations those test bring.

7.1 Parameterized tests

As described in section 3, to identify a signal we have to find the correct values for nine parameters using template banks (the mass of the individual black holes, the distance to the observer, the angular orrientation of the orbit, the angular orrientation with respect to the observer, the time of coalesence). This is done using matched filtering. As shown in [MTG+18], with a parameterized test we add an extra parameter that influences the value of a certain amplitude. In other words let $p(\bar{\theta})$ be an amplitude of a mode of the waveform which depends on some parameters. Then we define the extra parameter $\delta\hat{p}$. Then in our analysis we change

$$p(\bar{\theta}) \to (1 + \delta\hat{p})p(\bar{\theta}). \tag{7.1}$$

Then we can again try to match different waveforms with the incomming signal, but this time also allowing the parameter $\delta\hat{p}$ to vary. If general relatvity is indeed correct, then a waveform with $\delta\hat{p} = 0$ should give the highest match.

Recent results that were found using parameterized tests for the amplitudes to describe the phase of the wave [Aea20c]. These are the parameters that are also described in figure 10. By deviating some of these parameters they found that the observations agreed with general relativity.

7.2 Testing the relative amplitudes of the harmonics

Now that not just the dominant harmonic can be observed, but also the higher harmonics can be measured, we can use parameterized tests in a new way to test general relativity. We can define new parameters to deviate the amplitudes of the modes. Consequently, we can try to find waveform models that fit our measured data better.

For this process we define the parameters a_{lm}. These parameters will be added to the amplitudes of the modes. Our new waveform then becomes

$$h(t) = \sum_{l=2}^{3} \sum_{m=-l}^{l} (1 + a_{lm}) h^{lm}(t) \, {}_{-2}Y^{lm}(\theta, \varphi). \tag{7.2}$$

These parameters will take values between $[-3, 3]$ and will be included in the template bank. Furthermore, we will use the IMRPhenomHM waveform to test it against the data. By selecting different modes and adding them ourselves, we can get the waveforms that are described by eq. 7.2. These will then be tested against the signal.

Due to insufficient time to actually run the algorithm on the data, we will do a simplified version of the parameterized test. Namely we will only alter the inclination angle ι and the factor a_{lm} for all values of l and m except $l = 2$, $m = 2$. Furthermore, we will not match it with the data. Instead, we we match it with a waveform of constant inclination angle and $a_{lm} = 0$. In this way we still get a feeling for the process and how the algorithm works.

7.3 Sensitivity to deviations

If we would test our waveforms against the data then there are always deviations that we have to consider. These include inaccuracies caused by noise, or incompletness of the template bank. Therefore, we will always have an insecurity range for the determined values of parameters. If the value of $a_{lm} = 0$ for some l and m would be outside the margin of uncertainty, then we can doubt the validity of the theory.

First we will discuss what influence the noise may have on the outcome. Even though the noise is random, and we try to filter it out by integrating over longer times. It still influences the incomming signal. Therefore, another value for a parameter can give a higher match than the value that actually corresponds with the incomming signal. Consequently, we should consider all waveforms with a match above a certain boundary. This way we can be certain we do include the actual matching waveform.

Likewise, we are using template banks to spread the values of variables. This means that not all values of the parameters are considered. We will try to keep the value of the match between neighbouring points high enough, to not miss out on any matches that we miss. Nevertheless, it could still occur dat a point between neighbouring points gives a match much higher than the match at the two points. Therefore, we always should include a range around the points that gives the highest match as a margin of uncertainty.

8 Simulations

8.1 simulated signals

Now we will set up our parameterized test. First of all we will only change the value of a_{33}. Secondly, we will also alter the inclination angle ι. To do this we define a function in python that takes the $l = 2$, $m = 2$ and the $l = 3$, $m = 3$ modes of the IMRPhenomHM waveform and multiplies the amplitude of the $l = 3$, $m = 3$ mode by $(1 + a_{33})$. Next we add the two modes. It turns out that the match between the waveform we just created with $a_{33} = 0$ and the normal IMRPhenomHM waveform with the two modes called immediately, is 1. Therefore, this is a fine way to create the parameterized waveform.

In order to let the higher modes be of importance, we will choose $m_1 = 30\,M_\odot$ and $m_2 = 8\,M_\odot$. Aditionally, we choose values for the inclination angle uniform between $[0, \pi]$. For a_{33} we will take values between $[-3, 3]$. For our constant IMRPhenomHM waveform that we will compare the new waveform with, we take $\iota = \frac{50}{180}\pi$ and $a_{33} = 0$.

8.2 results

It turns out that both our tests give the expected result. As can be seen in figure 12, the match peaks for $a_{33} = 0$. Therefore, the model corresponds with itself. Likewise, in figure 13, we see the same happening. Furthermore, note how the graph widens for lower values of ι.

Additionally, we see that for when inclination angles of the two waveforms do not correspond, the match does not peak at $a_{33} = 0$. Instead, the peak transfers to higher values of a_{33}. This happens because when the value of ι gets closer to 0 or π, then the amplitude of the $l = 3, m = 3$ mode decreases. This has to be compensated by the a_{33} value to get a higher match.

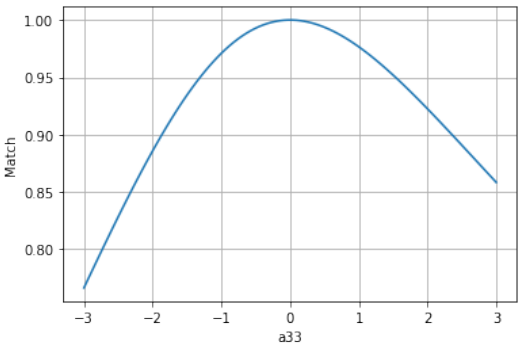

Figure 12: The match between the constant IMRPhenomHM waveform and the parameterized waveform. Here $\iota = \frac{\pi}{3}$, $m_1 = 30$ and $m_2 = 8$.

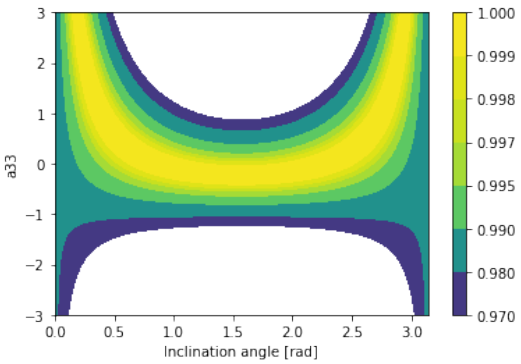

Figure 13: A contour plot of the match between the parameterized waveform and the constant IMRPhenomHM waveform. For the constant waveform $\iota = \frac{50}{180}\pi$. For both waveforms $m_1 = 30$ and $m_2 = 8$

9 Conclusion

In this thesis we have looked at higher harmonics that appear in gravitational waves that are generated by the merger of binary black holes. We have succeeded in calculating them up to 0.5 PN order. Using the linearized Einstein equations and by Taylor expanding the stress-energy tensor of the source, we were able to express the wave in terms of mass and momentum multipoles. We calculated these to finally find an expression for the waveform.

Furthermore, it turned out to be useful to express the waveform in terms of spin-weighted spherical harmonics. Using the transverse traceless gauge and its properties we were able to derive that the waveform can be expressed in terms of $\mathbf{T}^{E2,lm}$ and $\mathbf{T}^{B2,lm}$. Then, we also found a relation between these tensor harmonics and the spin-2 weighted spherical harmonics. This enabled us to express the waveform in terms of spin-2 weighted spherical harmonics. Finally, by using the stationary phase approximation giving us an expression for the phase, we completed the expression for the waveform:

$$\tilde{h}(f,\theta,\varphi) = \sum_{l=2}^{\infty} \sum_{m=-l}^{l} \tilde{h}^{lm}(f)\, {}_{-2}Y^{lm}(\theta,\varphi). \tag{9.1}$$

Additionally, we described algorithms and techniques to detect gravitational waves signals. We derived the properties of matched filtering, as well as those of nested sampling. Furthermore, we applied nested sampling on a simplified problem to understand how it works. We looked at the PyCBC library and how it could help us estimate the parameters for gravitational waves. In addition, we defined parameterized tests and looked at how we can test general relativity in a new way using this method.

Even though we did not have enough time to actually do the parameter estimation on the GW190814 and GW190412 data, we do have all the parts ready that we need. Instead, we did a simpler parameterized test, where we altered the amplitude of the $l = 3$, $m = 3$ mode, to see how parameterized tests work. We conclude that it is possible to test general relativity using the higher harmonics. We can test it because we know how to calculate the predictions done by general relativity, we know that we can measure the higher harmonics in the signals, and finally because we have tests and algorithms ready for use.

10 Discusion and outlook

Unfortunately, we were not able to test general relativity in this thesis due to insufficient time. Nevertheless, we have all the elements ready in this thesis. Therefore, this is surely something that needs to be done in future research.

It is quite a big step already that overtones can be measured in gravitational waves signals. However, in the future we hope to also be able to measure even higher overtones. Therefore, some possibilities for future research are:

1. Test general relativity using a parameterized test on the amplitude of the first overtones. These include the $l = 3$, $m = 3$ mode, the $l = 2$, $m = 1$ mode and the $l = 3$, $m = 1$ mode.

2. In the future when even higher PN orders can be observed, we can test general relativity on those amplitudes as well.

3. One could try to do a similar test, but for binary neutron stars instead of black holes.

4. One could do similar test for binary black holes with spin. Then we include spin parameters in the waveform as well, to analyse how this would influence the prediction.

However, most of these tests cannot take place until detectors are further improved. Still, since we have more and more data available to us and detectors keep on improving, maybe these test are possible in the near future.

References

[Aea20a] R. Abbott and et al. Gw190412: Observation of a binary-black-hole coalescence with asymmetric masses. *Physical Review D*, 102(4), Aug 2020.

[Aea20b] R. Abbott and et al. Gw190814: Gravitational waves from the coalescence of a 23 solar mass black hole with a 2.6 solar mass compact object. *The Astrophysical Journal*, 896(2):L44, Jun 2020.

[Aea20c] R. Abbott and et al. Tests of general relativity with binary black holes from the second ligo-virgo gravitational-wave transient catalog. 2020.

[BD99] A. Buonanno and T. Damour. Effective one-body approach to general relativistic two-body dynamics. *Physical Review D*, 59(8), Mar 1999.

[BPA16] et. al. B. P. Abbott. Observation of gravitational waves from a binary black hole merger. *Physical review letters*, 1(061102):1, 2016.

[BS10] Thomas W. Baumgarte and Stuart L. Shapiro. *Numerical Relativity: Solving Einstein's Equations on the Computer*. Cambridge University Press, 2010.

[GMN+67] J. N. Goldberg, A. J. Macfarlane, E. T. Newman, F. Rohrlich, and E. C. G. Sudarshan. Spin-s Spherical Harmonics and . *Journal of Mathematical Physics*, 8(11):2155–2161, November 1967.

[KAs18] B.S. Sathyaprakash K.G. Arun, Bala R Iyer and Prnaesh A sundararajan. Parameter estimation of inspiralling compact binaries using 3.5 post-newtonian gravitational wave phasing: The non-spinning case. *Raman Research institute, Bangalore, India*, 1(560080):6 – 7, 2018.

[Law18] E. Kidder Lawrence. Using full information when computing modes of post-newtonian waveforms from inspiralling compact binaries in circular orbit. *center for Radiophysics and Space Research, Cornell University, Ithaca, New York*, 1(14853):1 – 11, 2018.

[LB07] Michel Le Bellac. *Quantum Physics*. Cambridge University Press, University printing House, Cambridge CB2 8BS, United Kingdom, 2nd edition, 2007.

[Lea18] Lionel London and et al. First higher-multipole model of gravitational waves from spinning and coalescing black-hole binaries. *Physical Review Letters*, 120(16), Apr 2018.

[Mag08] Michele Maggiore. *Gravitation Waves Volume 1: Theory and Experiments*. Oxford University Press, Great Clarendon street, Oxford OX2 6DP, 1st edition, 2008.

[Mis16] Chandra Kant Mishra. Ready-to-use post-newtonian gravitational waveforms for binary black holes with non-precessing spins: An update. *International Centre for Theoretical Sciences-Tata Institute of Fundamental Research, Bangalore*, 1(560089):5 – 6, 2016.

[MTG+18] Jeroen Meidam, Ka Wa Tsang, Janna Goldstein, Michalis Agathos, Archisman Ghosh, Carl-Johan Haster, Vivien Raymond, Anuradha Samajdar, Patricia Schmidt, Rory Smith, and et al. Parametrized tests of the strong-field dynamics of general relativity using gravitational wave signals from coalescing binary black holes: Fast likelihood calculations and sensitivity of the method. *Physical Review D*, 97(4), Feb 2018.

[Pre05] Frans Pretorius. Evolution of binary black-hole spacetimes. *Physical Review Letters*, 95(12), Sep 2005.

[Tho80] Kip S. Thorne. Multipole expansions of gravitational radiation. *Reviews of Modern Physics*, 2(52):299–399, 1980.

[Tur60] G. Turin. An introduction to matched filters. *IRE Trans. Inf. Theory*, 6:311–329, 1960.

[Wig97] E. P. Wigner. *The Basic Conflict Between the Concepts of General Relativity and of Quantum Mechanics*. Springer Berlin Heidelberg, Berlin, Heidelberg, 1997.

[Zer70] Frank J. Zerilli. Tensor harmonics in canonical form for gravitational radiation and other applications. *Journal of Mathematical Physics*, 11(7):2203–2208, 1970.